UNIL | Université de Lausanne

Unicentre
CH-1015 Lausanne
http://serval.unil.ch

Year : 2018

Characterization of NOTCH signalling pathway in PTEN-deficient prostate tumorigenesis

Revandkar Ajinkya

Revandkar Ajinkya, 2018, Characterization of NOTCH signalling pathway in PTEN-deficient prostate tumorigenesis

Originally published at : Thesis, University of Lausanne

Posted at the University of Lausanne Open Archive http://serval.unil.ch
Document URN : urn:nbn:ch:serval-BIB_26421262ACA82

Droits d'auteur
L'Université de Lausanne attire expressément l'attention des utilisateurs sur le fait que tous les documents publiés dans l'Archive SERVAL sont protégés par le droit d'auteur, conformément à la loi fédérale sur le droit d'auteur et les droits voisins (LDA). A ce titre, il est indispensable d'obtenir le consentement préalable de l'auteur et/ou de l'éditeur avant toute utilisation d'une oeuvre ou d'une partie d'une oeuvre ne relevant pas d'une utilisation à des fins personnelles au sens de la LDA (art. 19, al. 1 lettre a). A défaut, tout contrevenant s'expose aux sanctions prévues par cette loi. Nous déclinons toute responsabilité en la matière.

Copyright
The University of Lausanne expressly draws the attention of users to the fact that all documents published in the SERVAL Archive are protected by copyright in accordance with federal law on copyright and similar rights (LDA). Accordingly it is indispensable to obtain prior consent from the author and/or publisher before any use of a work or part of a work for purposes other than personal use within the meaning of LDA (art. 19, para. 1 letter a). Failure to do so will expose offenders to the sanctions laid down by this law. We accept no liability in this respect.

UNIL | Université de Lausanne

Faculté de biologie et de médecine

Characterization of NOTCH signalling pathway in PTEN-deficient prostate tumorigenesis

Thèse de doctorat ès sciences de la vie (PhD)

présentée à la

Faculté de biologie et de médecine
de l'Université de Lausanne

par

Ajinkya Revandkar

Biologiste diplômé ou Master de Sussex University, Grande-Bretagne

Jury

Prof.Fabio Martinon, Président
Prof. Andrea Alimonti, Directeur de thèse
Prof. Arkaitz Carracedo, expert
Prof. Fabio Grassi, expert

Lausanne 2018

UNIL | Université de Lausanne
Faculté de biologie
et de médecine

Ecole Doctorale

Doctorat ès sciences de la vie

Imprimatur

Vu le rapport présenté par le jury d'examen, composé de

Président· e	Monsieur	Prof. Fabio **Martinon**
Directeur· rice de thèse	Monsieur	Prof. Andrea **Alimonti**
Experts· es	Monsieur	Dr Arkaitz **Carracedo**
	Monsieur	Dr Fabio **Grassi**

le Conseil de Faculté autorise l'impression de la thèse de

Monsieur Ajinkya Revandkar

Master of Science Sussex University, Grande-Bretagne

intitulée

Characterization of NOTCH signalling pathway in PTEN-deficient prostate tumorigenesis

Lausanne, le 7 mars 2018

pour le Doyen
de la Faculté de biologie et de médecine

Prof. Fabio Martinon

Acknowledgements

God Almighty (Sadguru), you made it all possible and continue making it for me in every which way.

This work wouldn't have been possible without the guidance and support of so many people. First and foremost, I want to thank my supervisor Prof. Andrea Alimonti for his tremendous support and guidance throughout this project and beyond. His inputs still remain unparalleled and instrumental. I also want to thank each and every member of Alimonti lab from past and present especially Dr. Alberto Toso, Maria Luna Perciato who helped me in this project. I take this occasion to thank all the members of IOR/IRB, especially the technicians of SPF animal facility who take care of mice and our work. I want to sincerely thank Pfizer company particularly, Nick Sonja for Gamma-secretase inhibitor and the funds to carry out the preclinical trials. Along with Pfizer (WI173087), I want to thank European Research Council (ERC) starting grant (261342) and ERC consolidator (683136), Josef Steiner Foundation, Helmut Horten Foundation and Krebsliga (KFS 3505-08-2014) grants.

I want to thank my PhD committee members Prof. Arkaitz Carracedo, Prof. Fabio Grassi and Prof. Sophie Martin for their valuable guidance and support so far and very generously, graciously accepting to be members of my PhD committee.

On a personal note, I want to thank my parents and all family members who have always believed in me, supported me through thick and thin and continue to endlessly love me and my passion for this field, with all the sacrifices without ever mentioning. Lastly, I want to say that this work might give me a degree but the real Doctors of Philosophy (PhD) in and of my life will always be my Mother and my Father.

Summary

Prostate cancer is a commonly diagnosed non-cutaneous malignancy and one of the leading causes of cancer-related deaths in men. Particularly, advanced prostate cancer is considered of high-risk with poor prognosis and survival. Several studies have identified that activation NOTCH pathway is associated with advanced stage of the disease and therapy-resistance in patients. However, the mechanism by which NOTCH pathway is activated in prostate cancer still remains unknown. Moreover, preclinical studies determining the therapeutic efficacy of NOTCH pathway inhibitors in prostate cancer is lacking. Here, in this study we show that loss of PTEN, a frequently altered tumour suppressor gene in prostate cancer, upregulates the expression of *ADAM17*, thereby activating NOTCH signalling in prostate tumours. Mechanistically, loss of PTEN triggers the accumulation of an oncogenic isoform of the transcription factor CUX1 that favours *ADAM17* transcription. Notably, over-expression of the oncogenic isoform of CUX1 (p110 CUX1) both *in vitro* and *in vivo* resulted in up-regulation of *ADAM17* and activation of NOTCH signalling. Using prostate conditional inactivation of both *Pten* and *Notch1* along with preclinical trials carried out in *Pten*-null prostate conditional mouse models, we demonstrate that *Pten*-deficient prostate tumours are addicted to the Notch signalling. Importantly, we demonstrate that pharmacological inhibition of

Notch pathway using g-secretase inhibitor promotes growth arrest and restricts tumour-invasiveness in both *Pten*-null and *Pten/Trp53*-null prostate tumours by triggering cellular senescence.

Taken together, our study describes a novel pro-tumorigenic network that links PTEN-loss to ADAM17 and NOTCH signalling in a PI3K-independent manner, thus providing the rationale for the use of NOTCH pathway inhibitors in advance prostate cancer patients.

Résumé

Le cancer de la prostate est une maladie non-cutanée et l'une des causes majeures de décès par cancer chez les hommes. Le cancer de la prostate à stade avancé a notamment un mauvais pronostic vital et un taux de survie très faible. Plusieurs études ont montré que la voie de signalisation NOTCH était associée à l'état avancé de la maladie et à la résistance thérapeutique chez les patients traités. Cependant, le mécanisme par lequel la voie de signalisation Notch est activée dans le cancer de la prostate reste méconnu. De plus, les études précliniques déterminant l'efficacité thérapeutique des inhibiteurs de la voie Notch sont absents dans le cancer de la prostate. Notre étude montre que la perte de PTEN, un gène suppresseur de tumeur fréquemment altéré dans le cancer de la prostate, augmente l'expression de *ADAM17*, et de ce fait active la voie NOTCH dans les tumeurs de la prostate. La perte de PTEN enclenche l'accumulation d'un isoforme oncogénique du facteur de transcription CUX1 permettant la transcription de *ADAM17*. Plus précisément, la surexpression de l'isoforme oncogénique de CUX1 (p110 CUX1) *in vitro* et *in vivo*, conduit à la surexpression de *ADAM17* et à la voie de signalisation NOTCH. A l'aide de la technique d'inactivation conditionnelle de *Pten* et *Notch* dans la prostate, ainsi que d'essais précliniques effectué dans les modèles murins knock-out du gène *Pten*, nous avons démontré que les tumeurs de la prostate déficientes en *Pten* étaient dépendantes de la voie de signalisation NOTCH. Nous avons notamment démontré que l'inhibition de NOTCH par un inhibiteur de γ -sécrétase, permettait l'arrêt de la croissance tumorale et limitait l'invasion tumorale dans les modèles murins knock-out *Pten* et *Pten/Trp53* du cancer de la prostate et ce en déclenchant la sénescence cellulaire. Notre étude décrit ainsi un nouveau réseau pro tumorigénique liant la perte de PTEN à ADAM17 et à la voie de signalisation NOTCH, de manière indépendante de la voie PI3K. Cette étude justifie ainsi l'utilisation d'inhibiteurs de la voie NOTCH pour les patients atteints du cancer de la prostate en stade avancé.

List of abbreviations

PTEN	Phosphatase and tensin homolog
ADAM17	Disintegrin And Metalloproteinase Domain-Containing Protein 17
CUX1	Cut Like Homeobox 1
PCa	Prostate Cancer
PSA	Prostate-specific antigen
DRE	Digital Rectal Examination
PIN	Prostatic intraepithelial neoplasia
LG-PIN	Low grade Prostatic intraepithelial neoplasia
HG-PIN	High grade Prostatic intraepithelial neoplasia
KRas	Kirsten Rat Sarcoma Viral Oncogene Homolog
Smad4	Mothers Against DPP Homolog 4
MAPK	Mitogen-Activated Protein Kinase
c-Myc	Avian Myelocytomatosis Viral Oncogene Homolog
Skp2	S phase kinase-associated protein2
PIP2	Phosphatidylinositol-4,5-bisulphate
PIP3	Phosphatidylinositol-3,4,5-trisulphate
PI3K	Phosphoinositide 3-kinase
mTOR	Mammalian Target of Rapamycin
PDK1	Pyruvate dehydrogenase Kinase1
BAD	BCL2 Associated Agonist Of Cell Death
FOXO	Forkhead box O1
GSK3	Glycogen Synthase Kinase 3
ENTPD5	Ectonucleoside triphosphate diphosphohydrolase 5
SREBP1C	Sterol-responsive element-binding protein 1C

GLUT4	Glucose transporter 4
PPARγ	Peroxisome proliferator-activated receptor-γ
PGC1α	PPARγ co-activator 1α
ANXA2	Annexin 2
CDC42	Cell division cycle 42
PAR6	Partitioning defective 6
aPKC	atypical PKC
EMT	Epithelia-Mesenchymal transition
HSCs	Haematopoetic Stem Cells
LICs	Leukaemia-initiating cells
MVP	Major vault protein
HAUSP	Herpesvirus-associated ubiquitin-specific protease
PLK1	Polo-like kinase1
AURKs	Aurora kinases
PICS	PTEN-loss induced cellular senescene
TGFb	Transforming growth factor b
BMP	Bone morphogenetic protein
EGF	Epidermal growth factor
NRR	Negative regulator region
LNR	Lin12-Notch repeats
NICD	Notch intracellular domain
RAM	RBPjκ association module
NLS	Nuclear localising sequence
RBPjκ	Recombination Signal Binding Protein For Immunoglobulin Kappa J Region
ANK	Ankyrin repeats

DSL	Delta/Serrate/LAG
DOS	Delta and OSM-11-like proteins
NEXT	Notch extracellular domain
GSEA	Gene set enrichment analysis
IHC	Immunohistochemistry
WB	Western blot
HES1	Hairy and enhancer of split 1
RT-PCR	Real-time polymerase chain reaction
MEFs	Mouse embryonic fibroblasts
AP	Anterior prostate
DLP	Dorsolateral prostate
VP	Ventral prostate
H&E	Haematoxylin and eosin
IF	Immunofluorescence
DECODE	DECipherment Of DNA elements
TF	Transcription factor
ChIP	Chromatin Immunoprecipitation
EV	Empty vector
GSI	Gamma-secretase inhibitor

Table of Contents

List of Figures

1. Introduction

1.1 Prostate cancer: a brief overview

Prostate cancer is one of the most common cancer-type and a leading cause of cancer-related deaths in men. As of 2017, American Cancer Society estimates nearly 161,360 new cases of prostate cancer with approximately 26,730 deaths related to prostate cancer[1]. A single most risk factor that is known to trigger prostate cancer is age. While there is a chance of 1 in 10,000 men younger than 40 years to develop prostate cancer, this risk is augmented to 1 in 7 by the age of 60[2]. This relationship between prostate cancer and age is likely due to multiple risk factors such as environmental, physiological, genetic and ageing-related consequences[3]. While prostate cancer is an age-related disorder, various processes known to initiate prostate tumorigenesis remain oxidative stress and DNA damage, genetic and epigenetic alterations, inflammation, genetic factors and telomere-shortening. Many of the risk factors for prostate cancer such as age, race and family history cannot be controlled, however, early detection and screening methods have made it easier to treat such cancers[4].

Prostate cancer can be detected early by a highly accessible blood test for prostate-specific antigen (PSA) and digital rectal examination (DRE). Patients with elevated levels of PSA, typically undergo biopsies in order to detect the presence of any potential prostatic tumour lesions. Histopathologically, prostate tissues obtained from such biopsies are graded according to the 'Gleason grades' from most-differentiated to least-differentiated (Low-grade to high-grade respectively) on the scale of 1 to 5[5]. A combination of Gleason grades from two most predominant patterns determines the Gleason score. Prostate tumours with a Gleason score between 2-4 are considered to be less aggressive, while the ones in the range of 7-10 accounts for the most aggressive ones[6,7]. Apart from the benefits of early diagnosis provided by PSA screening, most of which represent a latent or indolent form of the disease, it is still difficult to

distinguish between the ones that will eventually evolve into more aggressive forms. At present this poses an absolute need to develop better molecular and diagnostic markers and approaches

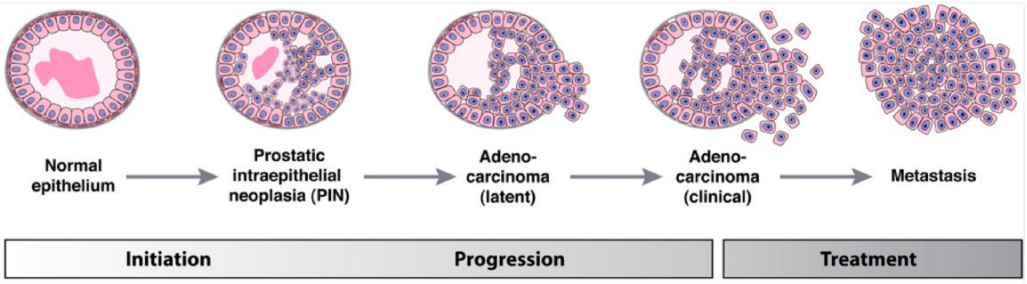

Image1: Stages of human prostate cancer progression

for effective management of prostate cancer along with the current histological analysis. Histopathological analysis of prostate biopsies still remains the major assessment criteria for prostate cancer to determine tumour grades and aggressiveness. Progression pattern for human prostate tumorigenesis is outlined in Image1[8].

Histologically, prostatic-intraepithelial neoplasia (PIN) is considered to be a precursor of prostate tumorigenesis prone/susceptible to evolve into an advanced form of the disease upon a combination of multiple aforementioned risk factors. While hyperplasia precedes PIN, PIN accounts for the pre-invasive stage of adenocarcinoma, preceding the onset of carcinoma by over 10 years[9]. PIN is mainly characterized by luminal epithelial hyperplasia, enlargement of nuclei, reduction in basal cells and nuclear atypia. Increase in the proliferative index of the tumour cells with these characteristics result in the development of high-grade PIN (HG-PIN)[10]. Studies using transgenic mouse models have successfully highlighted the role of several genetic alterations that result in development of PIN and subsequently prostate cancer. Some of these genetic alterations include complete loss of tumour suppressor genes such as *PTEN* and *Nkx3.1*[11,12,13]. Moreover, overexpression of proto-oncogene c-Myc in prostatic epithelia, mimicking its aberrant expression levels, is also known to drive PIN[14].

Most common type of prostate cancer corresponds to Adenocarcinoma, while mucinous carcinoma, signet-ring carcinoma and sarcoma are extremely rare forms of prostate cancer[15]. Adenocarcinoma, mainly of acinar type, has been distinguished into well-differentiated and poorly differentiated histological appearance[8]. In well-differentiated adenocarcinoma, most of the prostate glands lie in an irregular shape, loosely distributed in fibromuscular stroma with expansion in luminal cell compartment and reduction of basal cells[16]. Any stromal invasion of such glands is discernible and traceable while most of its structure remains intact. Basal membrane distinguishes tumour glands from stroma with no detectable necrosis[17]. On the other

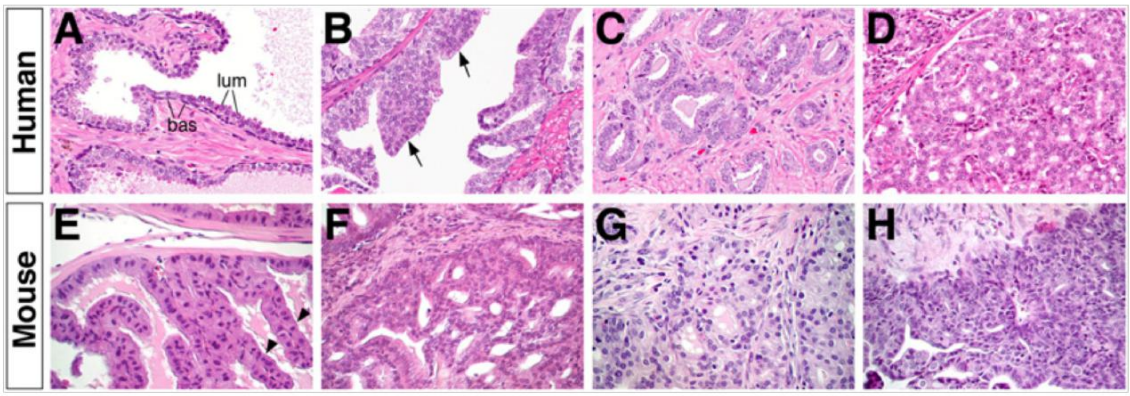

Image 2. Histopathological images of H&E stained human and mouse prostate tumour sections. (A) Benign human prostate tissue with basal (bas) and luminal (lum) cells. (B) PIN human prostate tissue, arrows indicating hyperplastic regions. (C) Well-differentiated adenocarcinoma tumour tissue. (D) Poorly-differentiated human prostate cancer tissue section. (E) Normal mouse prostate tissues with the arrows pointing papillary tufts. (F) High-grade PIN. (G) Mouse prostate carcinoma. (H) Invasive prostate carcinoma.

hand, poorly-differentiated form corresponds to no visible separation of glands from its surrounding stroma due to the complete invasion of epithelia-stroma. Gross destruction of prostatic tissue architecture is evident in most of the tumour areas with highly reactive stroma and inflammation (Image 2)[8].

The ultimate form of prostate carcinoma is the metastatic dissemination of prostatic tumour cells into the bloodstream and to distant organs. Although prostate cancer cells are reported to metastasize to lung, liver and pleura, the most frequent site of metastasis remains to be in bone, referred to as osteoblastic lesions[18,19]. Recent studies have highlighted the relevance of

circulating prostate tumour cells in clusters and their clinical implication on patients-survival[20,21]. Prostate tumours are generally considered to have both a multifocal and a highly heterogeneous nature. Often, primary tumours exhibit multiple histological foci comprising of diverse genetic alterations. However, contrary to the heterogeneity of prostate tumours, various molecular and cytogenetic analyses in multiple metastases in the same patient show clonal-relatability[22]. This is indicative of the monoclonal nature of the metastatic cells derived from the same heterogeneous prostate tumour, displaying a selective clonal advantage that occurs during tumour progression. Therefore, the factors that provide this clonal selection may emerge as an attractive or promising therapeutic target to treat patients of the rather 'untreatable' stage of this disease. The use of genetically engineered mouse models has significantly enhanced our understanding of different stages of the disease including the molecular mechanisms of metastasis[8]. One of the most frequently lost genes in advanced and metastatic prostate cancer is *PTEN*[23]. Loss of Pten alone gives rise to invasive adenocarcinoma however, its combination with other genetic alterations, such as mutation in *KRas*[24] and loss of *Smad4*[25], triggers the metastatic potential of these tumours. Interestingly, constitutive activation of MAPK pathway through *KRas* mutation or loss of *Smad4* alone does not lead to prostate carcinoma, suggesting a potential role of *Pten*-loss in initiating tumorigenesis.

1.2 *PTEN*-loss: a key genetic and molecular event in prostate cancer initiation and progression

PTEN is a tumour suppressor gene which is frequently lost or mutated in a variety of cancers, including prostate cancer which accounts for approximately 30% of prostate cancer patients[26]. Molecular and cytogenetic studies in the 1980s first revealed partial or complete loss of chromosome 10 in multiple cancers including prostate[27]. In 1997, *PTEN* was discovered to be one of the tumour suppressor genes located on chromosome 10q23 which is frequently altered

in sporadic tumours[28,29]. Following the discovery of *PTEN*, much of the emphasis has been in understanding its role in cell biology and the diverse processes that it controls[30]. PTEN is a principle negative regulator of phosphoinositide 3-kinase (PI3K) pathway through its catalytic phosphatase activity, wherein it dephosphorylates phosphatidylinositol-3,4,5-triphosphate (PIP_3) to phosphatidylinositol-4,5-bisphosphate (PIP_2)[31]. Upon loss of PTEN, excessive PIP3 at plasma membrane recruits and activates a subset of proteins, including PDK1 and AKT family members. AKT kinase is activated at two different residues which further activate the PI3K-AKT pathway[32]. Activated PDK1 phosphorylates AKT at Thr308 while mammalian target of rapamycin (mTOR) complex C2 (mTORC2) phosphorylates AKT at Ser473[33]. Activated AKT isoforms (AKT1, AKT2, and AKT3) phosphorylate up to nearly 100 substrates thereby driving cell proliferation, survival, metabolism, angiogenesis and cellular architecture. AKT activation primarily drives anti-

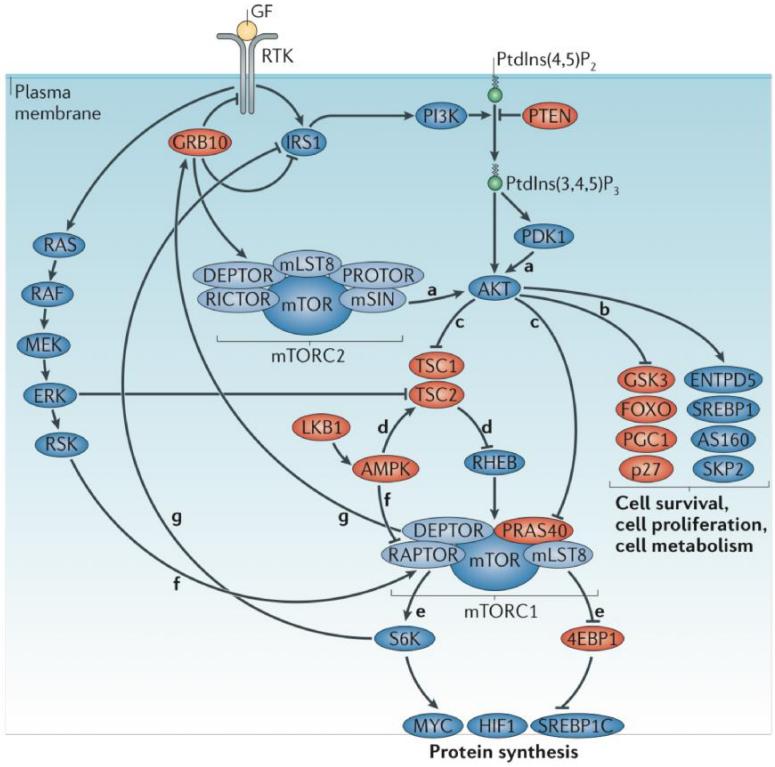

Image 3. PTEN-PI3K-AKT pathway. PTEN opposes PI3K function, thereby inhibiting AKT and mTOR pathway. PTEN-loss results in accumulation of PIP3 thereby recruiting PDK1 which phosphorylates AKT at Thr308 while mTORC2 phosphorylates AKT at Ser473. Activation of AKT leads to **a.** Cell survival, proliferation and cell metabolism through inhibition of GSK3, FOXO, PGC1 and p27 and through activation of ENTPD5, SREBP1, AS160 and SKP2 as in **b**. AKT also activates mTORC1 by mediating inhibitory phosphorylation of PRAS40 and TSC2 **c**. ERK is another kinase that phosphorylates and inhibits TSC2 thereby activating mTORC1 **d**. mTOR phosphorylates p70 ribosomal protein S6 kinase (S6K) and 4EBP1 to promote protein translation and survival **e**. Inhibition of mTORC1 can activate AKT by preventing negative feedback loop mediated by GRB10 and IRS1 **f, g**. Blue and red coloured molecules represent activators and repressors respectively.

apoptotic signals through inhibitory phosphorylation of BAD and Forkhead family proteins (FOXO), p27 and Glycogen synthase kinase 3 (GSK3). Secondly, active AKT also plays a role in activatory phosphorylation of series of proteins and protein complexes such as ectonucleoside triphosphate diphosphohydrolase 5 (ENTPD5), sterol-responsive element-binding protein 1C (SREBP1C), S phase kinase-associated protein 2 (SKP2) and mTORC1. Together, loss of PTEN through activation of PI3K-AKT pathway drive plethora of cellular responses which triggers diverse oncogenic signals[34].

Immediately after the discovery of *PTEN*-loss, generation of *Pten* knockout mice demonstrated the relevance of this tumour suppressor gene in multiple tissues. Over the past two decades, there have been several studies including the *Pten* transgenic mouse models to determine the functional role of PTEN. Some of the roles of PTEN as a tumour suppressor are outlined in brief below:

- *Cellular metabolism*: Emerging evidence suggests that during cancer initiation and progression metabolic reprogramming plays a key role in rapid cell proliferation. Rapidly proliferating cancer cells require an abundance of glucose which is readily converted into lactate through anaerobic glycolysis regardless of the presence of oxygen[35]. Loss of PTEN is known to drive high rates of glycolysis, increased biosynthesis of macromolecules such as lipids and enhanced lactate production. Insulin-mediated glucose uptake and membrane translocation of glucose transporter GLUT4 are enhanced by loss of PTEN and activation of the PI3K-AKT pathway[36]. PI3K–AKT signalling inhibits gluconeogenesis through blocking FOXO and peroxisome proliferator-activated receptor-γ (PPARγ) co-activator 1α (PGC1α)[37,38]. Furthermore, loss of PTEN activates the key lipogenic [38]transcription factor SREBP1C thereby activating lipogenesis[39]. Moreover, PTEN-loss also promotes protein glycosylation and folding through ENTPD5 in the endoplasmic reticulum (ER)

which further increases ATP consumption[40]. While dietary restriction might inhibit PI3K-AKT activity, loss of PTEN or PI3K mutations displays resistance to such effects.

- *Cell motility and polarity*: PTEN is mainly localized to the apical plasma membrane during epithelial morphogenesis, catalysing the conversion of PIP3 to PIP2 and recruiting Annexin 2 (ANXA2). Subsequently, CDC42 gets recruited to the plasma membrane and binds to partitioning defective 6 (PAR6)– atypical PKC (aPKC) complex to promote establishment of polarity[41]. Therefore, PTEN-loss may prevent normal development of apical surface and lumen. Thus, deregulation of PTEN-PI3K pathway may cause loss and gain of certain cellular characteristics such as loss of epithelial characteristics thereby increasing possible gain of mesenchymal properties allowing the EMT and increased cell motility[42].
- *Cancer stem cells*: Studies in understanding the role of PTEN in leukaemia and leukaemogenesis have shown that loss of PTEN causes depletion of Haematopoetic Stem Cells (HSCs) followed by generation of Leukaemia-initiating cells (LICs) promoting leukaemogenesis[43,44]. Treatment of rapamycin restored HSCs and thereby blocked the generation of LICs. These data highlighted the involvement of mTOR as a key mediator of this process. In addition to loss of PTEN, activation of b-catenin and recurring t (14;15) chromosomal translocation were also identified to cooperate and contribute to PTEN-deficient Leukaemogenesis[45]. Molecular insights revealed distinction between HSCs and LICs, and depending upon the PTEN status, specific targeted therapies can be designed to target PTEN pathway to suppress LICs.

- *In nucleus*: Several evidences demonstrate the nuclear role of PTEN protein and absence of which is associated with aggressive cancers. Given that PTEN plays a catalytic role on the membrane, its role in nucleus implies beyond its lipid phosphatase activity[46]. Numerous studies have defined critical functions of nuclear PTEN in genomic stability and cell cycle progression. Nuclear PTEN regulates DNA repair

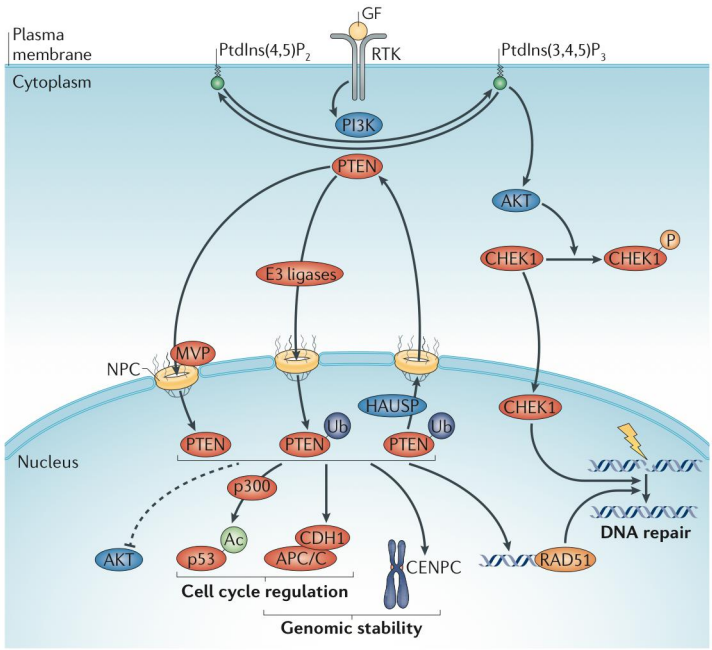

Image 4. Functional role of PTEN in the nucleus. Various processes lead to nuclear import of PTEN. Major vault protein (MVP)-mediated import is outlined which is dependent on monoubiquitylation of PTEN by E3 ubiquitin ligases. This process can be reversed upon deubiquitylation by (DUB) herpesvirus-associated ubiquitin-specific protease (HAUSP) that results in PTEN nuclear export. In the nucleus, PTEN binds to APC/C and CDH1 to promote tumour suppression. PTEN in nucleus also promotes genomic stability by binding to CENPC and RAD51. In addition, PTEN induces p53 acetylation in response to DNA damage to inhibit cell proliferation through p300.

through upregulation of RAD51which is involved in double-stranded break (DSB) repair[47]. Moreover, PTEN loss results in homologous recombination defects in human tumour cells. Importantly, nuclear PTEN is shown to promote APC/C association with CDH1 thereby enhancing E3 ligase activity of APC/C. This eventually promotes tumour suppression due to effective degradation of polo-like kinase1 (PLK1) and aurora kinases (AURKs) mediated by APC/C-CDH1 complex formation[48,49]. Altogether, these data indicate the phosphatase-independent activity of PTEN as a tumour suppressor in cells.

- *Cellular senescence*: Cellular senescence is an irreversible cell cycle arrest that occurs during natural ageing, process due to telomere erosion upon cellular divisions, referred

to as replicative senescence, or in response to diverse cellular stresses, known as premature senescence[50]. One such premature senescence is elicited upon complete loss of PTEN, termed PTEN-loss induced cellular senescence (PICS). This is a novel type of senescence response, unlike OIS, which is characterised by absence of both hyper proliferation and DNA damage response[51]. Complete loss of PTEN at early stage of tumour is associated with p53-dependent cellular senescence that reduces the tumour growth; however, upon concomitant loss of p53 drives rapid tumour progression[52]. In PICS, p53 is upregulated mainly through translation driven by mTORC1. However, unlike in OIS, where p53 is mainly activated and stabilized by $p19^{ARF}$, PICS doesn't rely on $p19^{ARF}$ for p53 stability[53]. Furthermore, concomitant loss of PTEN and transforming growth factor b (TGFb) – bone morphogenetic protein (BMP) – SMAD4 results in PICS bypass, enhancement of tumour cell proliferation and metastasis *in vivo*[25]. Moreover, concomitant loss of Pten and several other genetic events such as overexpression of proto oncogene *c-Myc*[14,54], activation of *KRas*[24], loss of tumour suppressor *Nkx3.1*[12] and oncogenic *TMPRSS2-ERG*[55] fusion is also known to promote prostate tumour progression.

Apart from activation of PI3K-AKT pathway, PTEN-loss is also involved in activation of several signalling pathways such as RAS-MAPK, JNK and RAC pathways[56]. Since it has been reported that Notch pathway is frequently altered in advanced PCa and loss of PTEN is also observed in the advance stage of the disease we aimed to determine the cross-talk between the two pathways.

1.3 Notch signalling pathway

Notch signalling pathway is a highly conserved signalling pathway during evolution and plays a critical role in development and tissue homeostasis. Since activated Notch pathway controls

diverse cellular and molecular processes, its role remains multifaceted and highly context specific. While Notch pathway has far-reaching impact on development and homeostasis, aberrant activation of this pathway is reported to initiate tumorigenesis and tumour progression[57]. The molecular mechanism of Notch pathway activation is discussed as below.

Notch receptors: Notch receptors are type1 transmembrane proteins which are expressed as four paralogs in mammals (Notch1-4)[58]. Each of these cell surface receptors comprises of three structural domains such as extracellular domain, single transmembrane domain, and intracellular domain. Extracellular domain consists of 29-36 tandem Epidermal growth factor (EGF)-like repeat proteins of which some may interact with the Notch ligands. Interaction with

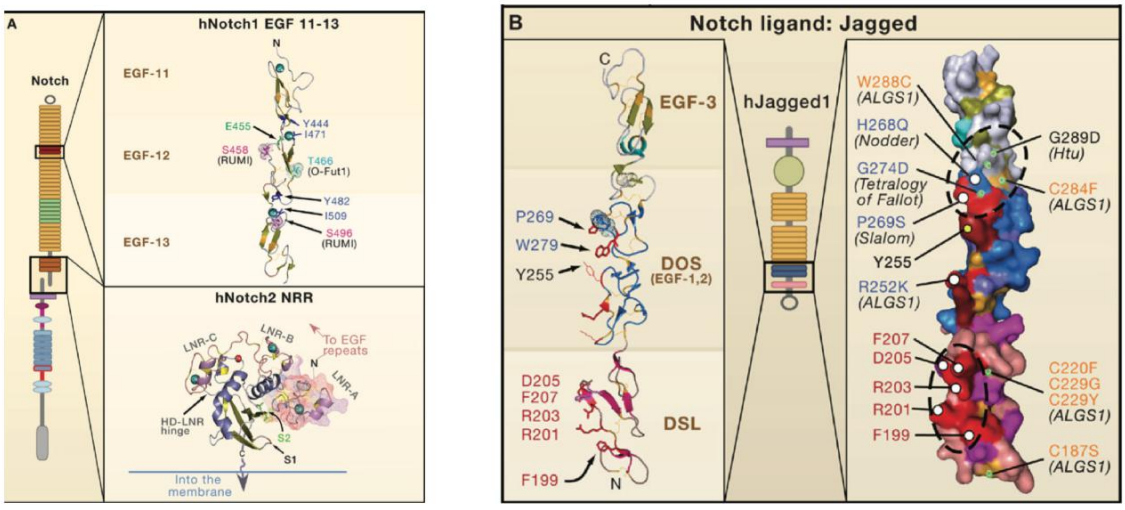

Image 5. Atomic resolution of Notch ligand and receptor. (**A**) Notch receptor with ligand binding domain containing EGF (11-13) centred by EGF repeat 12 which is suggested to interact with Jagged1 ligand on basis of computational docking models. (**B**) Notch ligand (Jagged) containing DSL, DOS and EGF repeat 3 domains. DSL domain, unlike EGF repeats contains regions in red that interact with Notch receptor.

the ligands presented on the neighbouring cells is mediated by 11-12 proteins of the receptor EGF-like region which is called *trans* interaction. Whereas, an inhibitory interaction that occurs between the receptor and the ligand expressed on the same cell, mediated by 24-29 repeats, is called *cis* interactions[59,60]. EGF repeats are followed by a unique negative regulator region (NRR) composed of three cysteine-rich Lin12-Notch repeats (LNR) and heterodimerization domain (HD)[57]. Upon translation, Notch receptor protein is glycosylated by O-fut and Rumi, a central process for production of functional receptor. The mature form

of the receptor is proteolytically cleaved by PC5/furin at site S1 which is eventually assembled together as a functional protein on the cell surface[61]. Single transmembrane domain comprises of a sequence terminated with 'translational stop' signal of 3-4 Arg/Lys residues. The Notch intracellular domain (NICD) consists of RBPjκ association module (RAM) that forms a high affinity binding module of 12-20 amino acids centred around a WxP module which is conserved motif. A long linker protein containing one nuclear localising sequence (NLS) links the RBPjκ association module (RAM) to the seven Ankyrin repeats (ANK) domain. Most ligands for the Notch receptors are type 1 transmembrane proteins, broadly presented mainly on neighbouring cells. Mainly, these ligands are structurally classified into three major protein domains: a. N-terminal Delta/Serrate/LAG-2 (DSL) motif, b. Specialized tandem EGF repeats called DOS domain (Delta and OSM-11-like proteins) and c. EGF-like repeats. While both DSL and DOS are involved in binding Notch receptor, DSL is reported to bind receptors during both *trans* and *cis* interactions. In addition, DSL ligands are classified into two categories mainly based on the presence (Jagged/Serrate) or absence (delta-like) of a cysteine-rich domain[57].

Notch-signalling pathway:

Canonically, Notch pathway is activated upon its interaction with the membrane-bound ligands on the surface of the neighbouring cells. Upon ligand-receptor interaction, a series of proteolytic cleavages within the Notch receptor triggers the release of intra-cellular domain of Notch to the nucleus where it functions as transcriptional activator. Hierarchically, ligand binding leads to cleavage of Notch receptor by ADAM metalloprotease at site S2 which is nearly 12 amino acids before transmembrane domain within NRR region. Notch ligand-receptor binding causes the 'open' conformation of receptor due to mechanical 'pull' in the direction of ligand-presenting cell. The open conformation allows the ADAM metalloproteases to access the inaccessible S2 cleavage site and generate ectodomain shredding leaving Notch

extracellular domain (NEXT)[62]. This ectodomain shredding is prerequisite for subsequent receptor cleavage and Notch pathway activation. While certain mutations in Notch HD domain are reported in human malignancies, such as T-ALL, that may cause a constitutively 'open' conformation[63], high amount of ADAMs may also result in Notch activation in a ligand-independent manner.

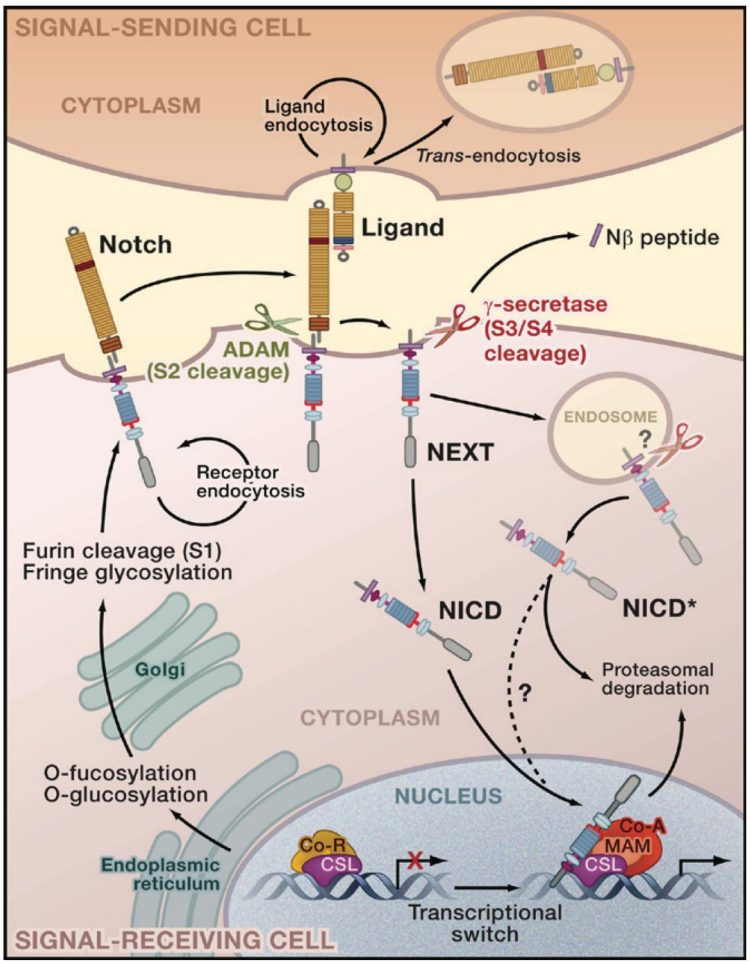

Image 6. Notch signalling pathway. A representation of series of proteolytic cleavages that leads to activatation of Notch signalling in cells. S1cleavage of the mature form of Notch receptor allows the assembly of the ligand and its presentation on the cell surface. S2 cleavage of extracellular fragment generating NEXT fragment. This results in S3 cleavage mediated by GS complex resulting in release of NICD1 fragment in the nucleus. Nuclear NICD1 triggers transcription of Notch target genes by forming a complex with CSL, Co-A and MAML. The same complex in absence of NICD1 act as transcriptional repressor of these genes.

Upon S2 cleavage, an enzyme complex, named g-secretase complex, is activated that mediate S3 cleavage on NEXT receptor in transmembrane domain (TMD) permitting the release of Notch intracellular domain (NICD) in the nucleus[64]. The g-secretase complex mainly consists of four subunits Presenilin1 (PSEN1), Nicastrin (NCT), Presenilin enhancer 2 (PEN2) and Anterior pharynx-defective1 (APH1)[65]. The S3 cleavage is mainly catalysed by the catalytic subunit of g-secretase complex, namely Presenilin (PSEN1), mediating NICD1 protein domain release from Val1744[66]. NICD upon translocation in the nucleus acts as a transcriptional activator of several genes, however, it is unable to bind the

DNA on its own. NICD binds to the DNA with help of a DNA-binding protein CSL (CBF1/ RBPjκ/Su(H)/Lag-1) via its RAM domain. The ANK domain of NICD recruits the coactivator Mastermind/Lag-3 (MAML). Mastermind recruits the MED8 mediator complex thereby leading to the upregulation of downstream target genes. While NICD binding to CSL is known to activate expression of Notch-target genes, in absence of NICD, these genes remain repressed due to the presence of CSL which functions as transcriptional repressor[67].

Several reports have highlighted the role of activated NOTCH signalling pathway in advanced and metastatic prostate cancer, which is also associated with frequent loss of PTEN. Thus, we aimed to determine the cross-talk between NOTCH pathway and PTEN/PI3K/AKT pathway in this study.

2. Results:

Pten-loss triggers activation of Notch signalling pathway in prostate cancer

To better understand the relevance of NOTCH signalling pathway as a consequence of loss of

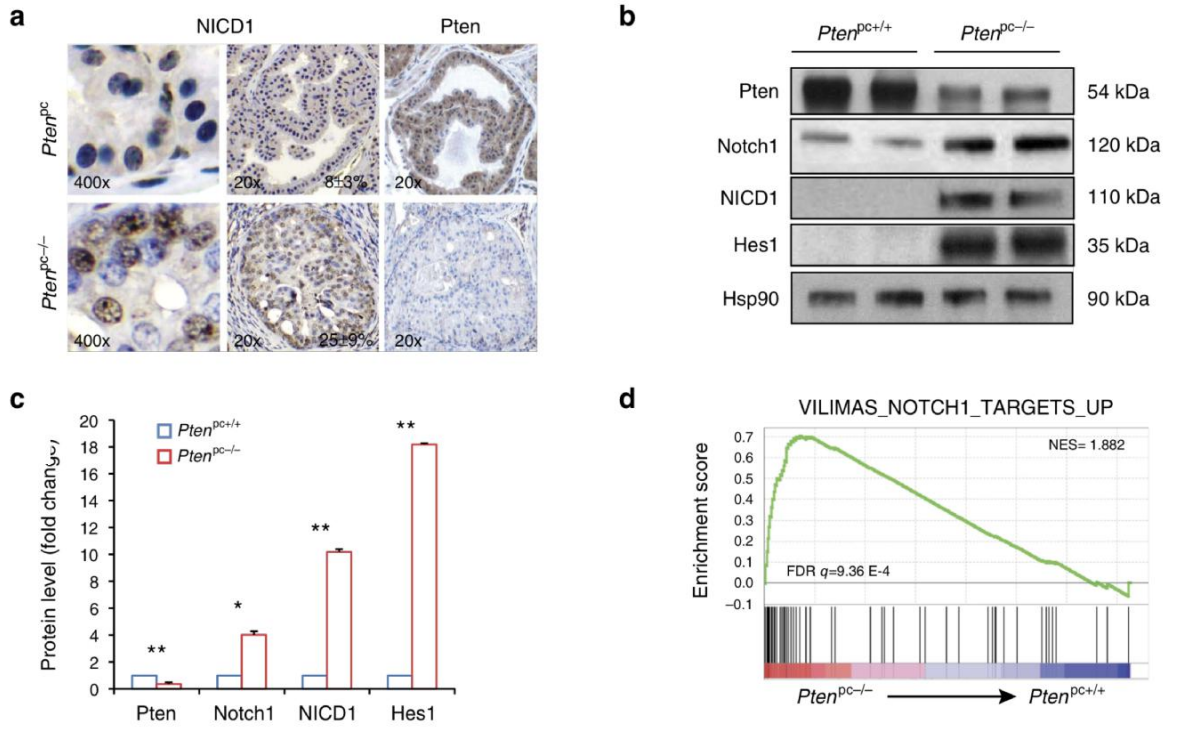

Fig 1. **Notch1 signalling is activated in *Pten*$^{pc-/-}$ prostate tumours.** (**a**) IHC showing NICD1 and Pten stainings in both *Pten*$^{pc+/+}$ normal prostate (8±3%) and *Pten*$^{pc-/-}$ prostatic intraepithelial neoplasia (PIN) lesions resected from 12-week-old mice (25±9%) (n=3) . Magnification 20x and 400x. (**b**) WB showing the protein levels of Pten, total Notch1, NICD1 and Hes1 in both *Pten*$^{pc+/+}$ prostate and *Pten*$^{pc-/-}$ prostate tumours (n=5). (**c**) Quantification of **b**. (**d**) Gene Set Enrichment Analysis (GSEA) showing activation of Notch1 signalling in *Pten*$^{pc-/-}$ prostate tumours.

PTEN in prostate cancer, we took an advantage of *Pten* prostate conditional mouse model (hereafter referred as *Pten*$^{pc-/-}$)[52]. At 12 weeks of age, *Pten*$^{pc-/-}$ mice showed a marked increase in Notch intracellular domain 1 (NICD1), a marker of Notch pathway activation[68], as observed by Immunohistochemical (IHC) and western blot (WB) analysis (Fig 1a-c). Consistently with these evidence, Gene Set Enrichment Analysis (GSEA) revealed a Notch signature in *Pten*$^{pc-/-}$ prostate tumours (Fig 1d). In addition, a human PCa data set also validated these results showing an inverse correlation between *PTEN* and *HES1* (a downstream target of Notch1

pathway) mRNA levels (Fig 2a). Given the activation of Notch1 pathway in *Pten*$^{pc-/-}$ prostate

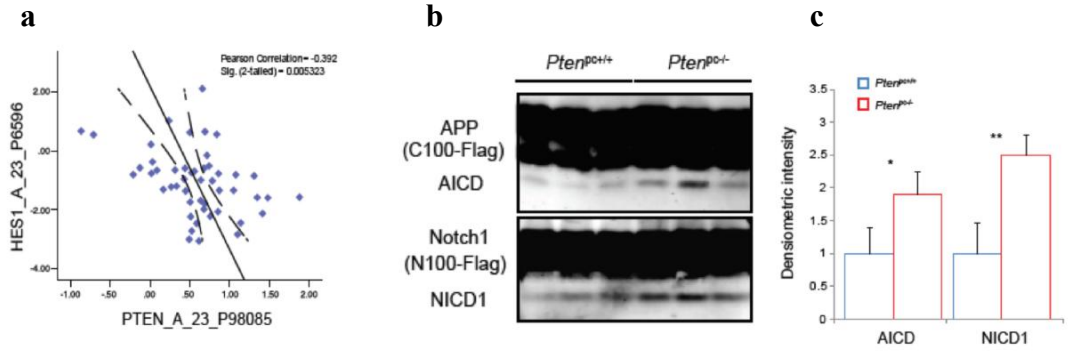

Fig 2. **Notch pathway activation observed in PTEN-deficient prostate tumours in patients and mouse models.** (**a**) Inverse correlation between PTEN and HES1 mRNA levels in a human prostate cancer dataset. (**b**) Enzymatic *in vitro* assay showing the elevated activity of the g-secretase complex in *Pten*$^{pc-/-}$ prostate tumours (n=3). (**c**) Quantification of **b**.

tumours, we aimed to determine the role of g-secretase enzyme complex, a key mediator of intracellular Notch receptor cleavage that subsequently leads to the pathway activation.

Enzymatic activity assay showed enhanced g-secretase complex activity in *Pten*$^{pc-/-}$ prostate tumours compared to age-matched *WT* prostates (Fig 2b-c). These data conclusively explained the intracellular receptor shredding subsequently activating Notch1 pathway upon loss of *Pten*. Taken together, these results demonstrate that loss of PTEN activates NOTCH signalling in prostate tumours.

Combined genetic inactivation of *Notch1* and *Pten* promotes tumour inhibition and senescence activation

To evaluate the relevance of Notch1 signalling in *Pten*$^{pc-/-}$ prostate tumours, we generated a conditional concomitant knockout of *Pten* and *Notch1* in prostatic epithelium. At first, we confirmed the prostate-specific deletion of both *Pten* (by western blot) and *Notch1* (for its target genes by RT-PCR) (Fig 3a). To obtain the genetic evidence of how a combined loss of *Notch1* and *Pten* affects the murine prostate tumorigenesis, we performed a histopathological analysis. Mice at different ages were sacrificed and the prostates were resected from *Pten*$^{pc+/+}$,

Notch1$^{pc-/-}$, *Pten*$^{pc-/-}$ and *Pten*$^{pc-/-}$; *Notch1*$^{pc-/-}$. Notably, genetic inactivation of *Notch1* in *Pten*$^{pc-/-}$ prostate tumours triggered a strong inhibition of tumour growth compared to the age-matched *Pten*$^{pc-/-}$ littermates. This evidence was evaluated based on the decreased number of glands

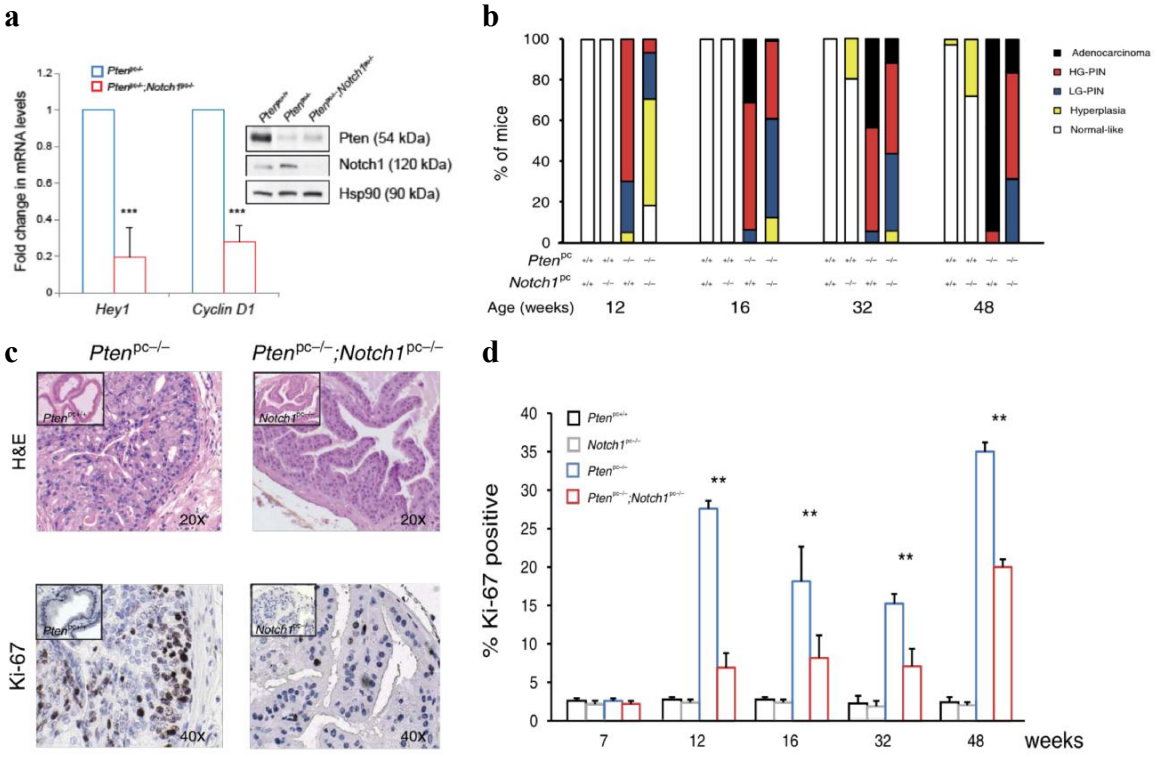

Fig 3. **Combined genetic inactivation of *Pten* and *Notch1* delay prostate tumorigenesis.** (**a**) Fold change in mRNA levels of *Hey1* and *Cyclin D1* target genes of Notch pathway in *Pten*$^{pc-/-}$; *Notch1* $^{pc-/-}$ tumours compared to *Pten*$^{pc-/-}$ tumours. WB showing the protein level of Pten and Notch1 in *Pten*$^{pc+/+}$, *Pten*$^{pc-/-}$ and *Pten*$^{pc-/-}$; *Notch1*$^{pc-/-}$ prostate tumours. (**b**) Histopathological characterization of normal prostates and prostate tumours in mice of the indicated genotypes (n=16 for each genotype). (**c**) H&E and Ki-67 staining of APs derived from 12-week-old *Pten*$^{pc-/-}$ and *Pten*$^{pc-/-}$; *Notch1*$^{pc-/-}$ tumours (n=5). Magnification 20x and 40x, respectively. Insets represent H&E and Ki-67 images of *Pten*$^{pc+/+}$ and *Notch1*$^{pc+/+}$. (**d**) Quantification of Ki-67 staining of APs in mice of indicated genotypes.

affected by high-grade prostatic intraepithelial neoplasia (HG-PIN) and invasive PCa (Fig 3b). Furthermore, *Pten*$^{pc-/-}$; *Notch1*$^{pc-/-}$ tumours showed reduced cell proliferation observed by decreased Ki67 staining (a marker of cell proliferation) as compared to the age-match *Pten*$^{pc-/-}$ tumours (Fig 3c-d). Of note, neither *Pten*$^{pc+/+}$ nor *Notch1*$^{pc-/-}$ developed any prostatic lesions (Fig 3c-d). Intriguingly, we observed a strong increase in p27 protein levels, a marker of senescence response, in *Pten*$^{pc-/-}$; *Notch1*$^{pc-/-}$ tumours compared to *Pten*$^{pc-/-}$ tumours (Fig 4a, b).

These genetic evidence suggest an oncogenic role of *Notch1* in *Pten*-null tumours and that loss of *Notch1* can delay the tumorigenesis.

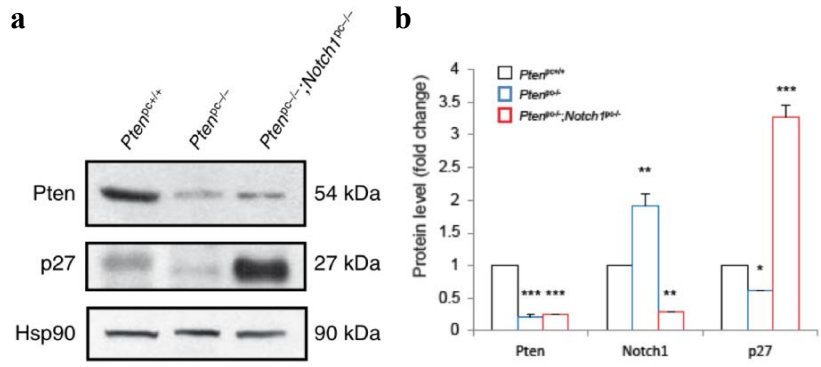

Fig 4. Inactivation of Notch1 in Pten null tumours elicit p27 driven senescence response. (**a**) WB showing the protein levels of Pten and p27 in *Pten*$^{pc+/+}$, *Pten*$^{pc-/-}$ and *Pten*$^{pc-/-}$; *Notch1*$^{pc-/-}$ prostate tumours. (**b**) Quantification of **a**.

PF-03084014, a potent g-secretase inhibitor, restricts tumour progression by promoting p27-driven senescence response in advanced PCa

As guided by the genetic evidence, we questioned whether pharmacological targeting of Notch pathway could also induce similar response in advanced PCa. Therefore, we tested a potent g-

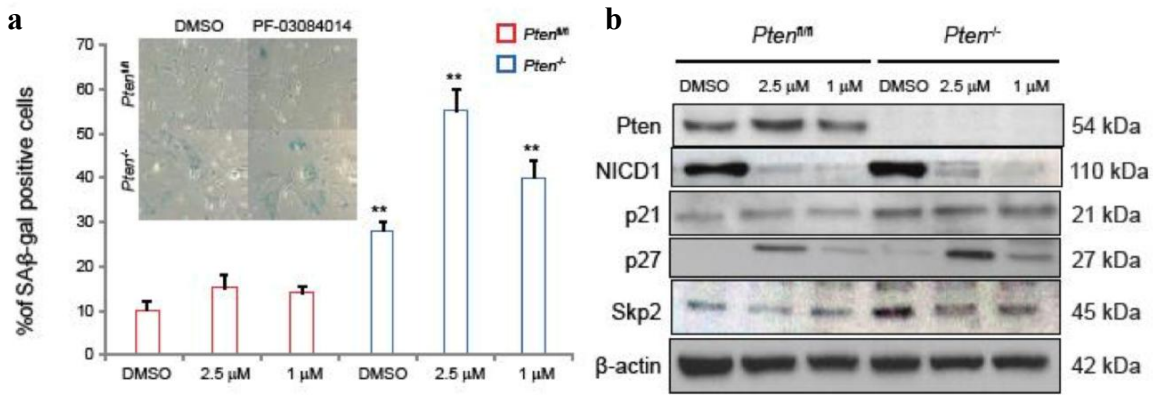

Fig 5. Pharmacological targeting of Notch pathway using PF-03084014 triggers senescence in Pten-null MEFs. (**a**) SA-b-gal assay in Ptenfl/fl and Pten-/- MEFs after treatment with PF-03084014 at 2.5μm and 1μm. (b) WB showing effect of PF-03084014 on the protein levels of NICD1, p21, p27 and the Notch1 target gene Skp2.

secretase inhibitor, PF-03084014 (currently under clinical evaluation)[69,70] , in *Pten*-null mouse embryonic fibroblasts (MEFs). Treatment of *Pten*$^{-/-}$ MEFs with PF-03084014 showed significant increase in both p27 protein levels and senescence-associated beta-galactosidase

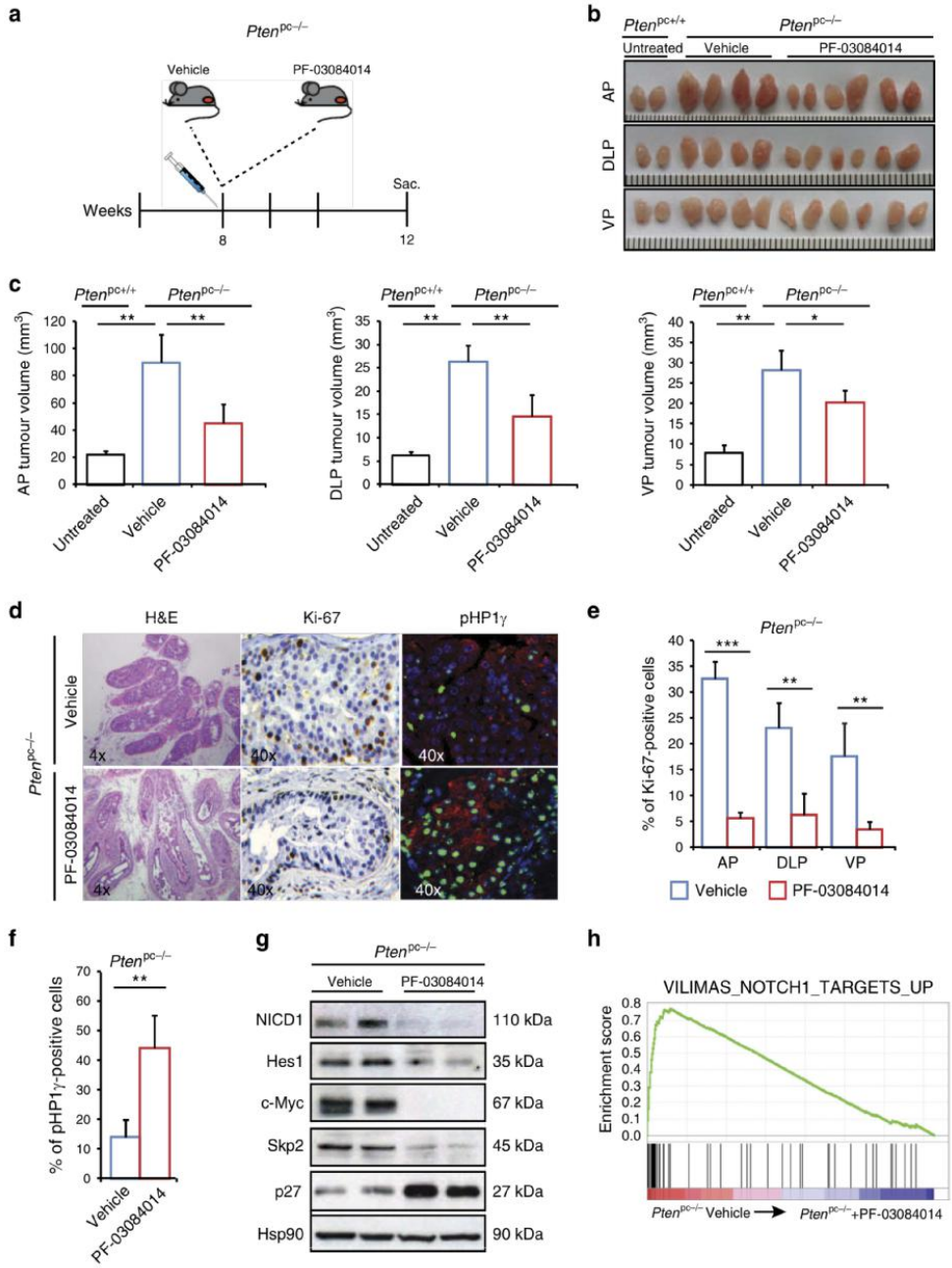

Fig 6. PF-03084014 constrains tumorigenesis of *Pten*$^{pc-/-}$ prostate tumours. (**a**) Scheme of treatment. Mice have been treated twice a day for 4 weeks with either vehicle or PF-03084014 (100 mg/kg). (**b**) Picture showing the size of anterior (AP), dorso-lateral (DLP) and ventral prostates (VP) from *Pten*$^{pc+/+}$ WT prostates and *Pten*$^{pc-/-}$ tumours treated with either vehicle or PF-03084014. (**c**) Quantification of **b** (n=5). (d) H&E, Ki-67 and pHP1g staining of APs derived from *Pten*$^{pc-/-}$ tumours treated with either vehicle or PF-03084014. Magnification 4x and 40x. (**e,f**) Quantification of **d** (n=5). (**g**) WB on AP extracts *Pten*$^{pc-/-}$ tumours showing the effect of PF-03084014 on Notch1 signalling. (**h**) Gene Set Enrichment Analysis (GSEA) showing reduced Notch1 signalling in *Pten*$^{pc-/-}$ prostate tumours treated with PF-03084014. Values are expressed as mean±s.e.m. *P<0.05; **P<0.01; ***P<0.001 by Student's t-test.

(SA-b-gal) activity, two markers of senescence, at low doses (2.5μm to 1μm) (Fig 5 a, b). This

data prompted us to determine the *in vivo* efficacy of PF-03084014 using *Pten*$^{pc-/-}$ transgenic

mice as a proof-of principle for pharmacological targeting Notch pathway in treating PCa. Having demonstrated the significance of Notch1 pathway activation genetically in prostate tumours and pharmacologically *in vitro* using PF-03084014, we next set-up a

*Pten*pc-/-

preclinical trial in *Pten*$^{pc-/-}$ transgenic mice to determine the anti-tumour efficacy of g-secretase inhibitor *in vivo*. We treated a cohort of *Pten*$^{pc-/-}$ mice at 8-weeks of age, at the onset of tumour

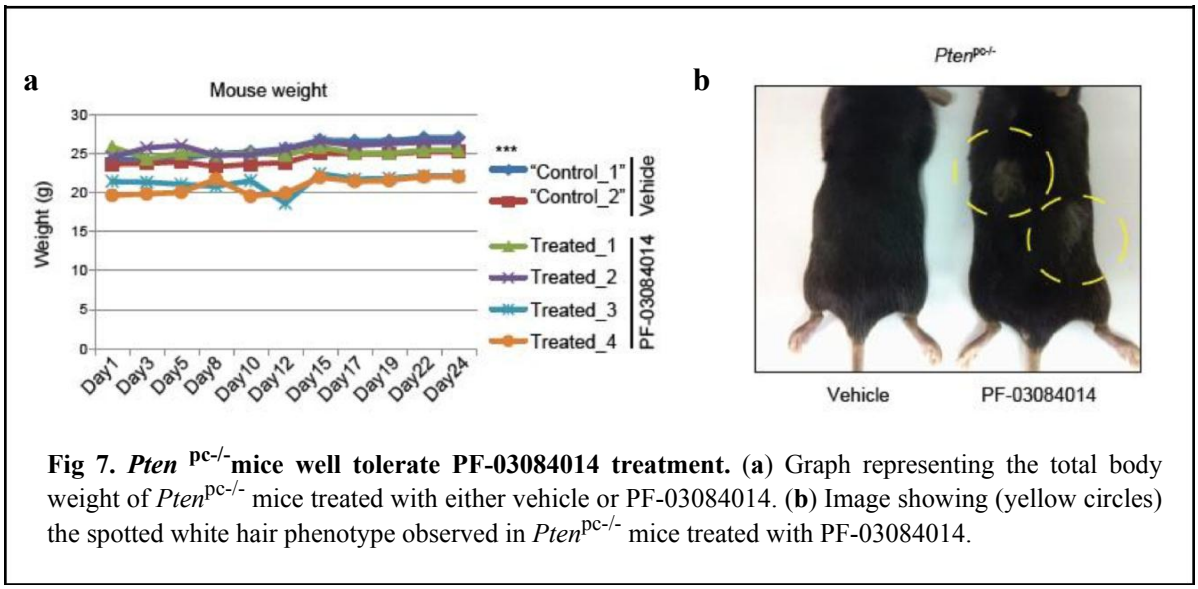

Fig 7. *Pten* $^{pc-/-}$mice well tolerate PF-03084014 treatment. (**a**) Graph representing the total body weight of *Pten*$^{pc-/-}$ mice treated with either vehicle or PF-03084014. (**b**) Image showing (yellow circles) the spotted white hair phenotype observed in *Pten*$^{pc-/-}$ mice treated with PF-03084014.

development, with PF-03084014 for a total of 20 days (Fig 6a). At the end of the treatment, mice were euthanized and the prostates were resected for analysis. Gross anatomy of the prostate lobes revealed a significant decrease in tumour size in *Pten*$^{pc-/-}$ mice treated with PF-03084014 compared to the control (Fig 6b, c). Decrease in tumour size was associated with reduction in cell proliferation as determined by Ki67 staining and increase in senescence, as

determined by pHP1g staining and p27 protein levels (Fig 6d-f). Interestingly, we found reduction in the protein levels of S-phase kinase-associated protein 2 (Skp2), an inhibitor of p27 (Fig 6g)[53]. Reduced levels of NICD1 and Notch target genes confirmed that PF-03084014 efficiently reached the target (Fig 6g). Furthermore, GSEA analysis confirmed the decrease in Notch signalling pathway in *Pten*$^{pc-/-}$ tumours upon treatment with PF-03084014 (Fig 6h). PF-03084014 was well tolerated with no significant evidence of total body weight loss and normal

behavioural patterns observed as per the state guidelines (Fig 7a). While mice treated with PF-03084014 did not show any signs of distress or toxicity, we observed a spotted loss-of-hair

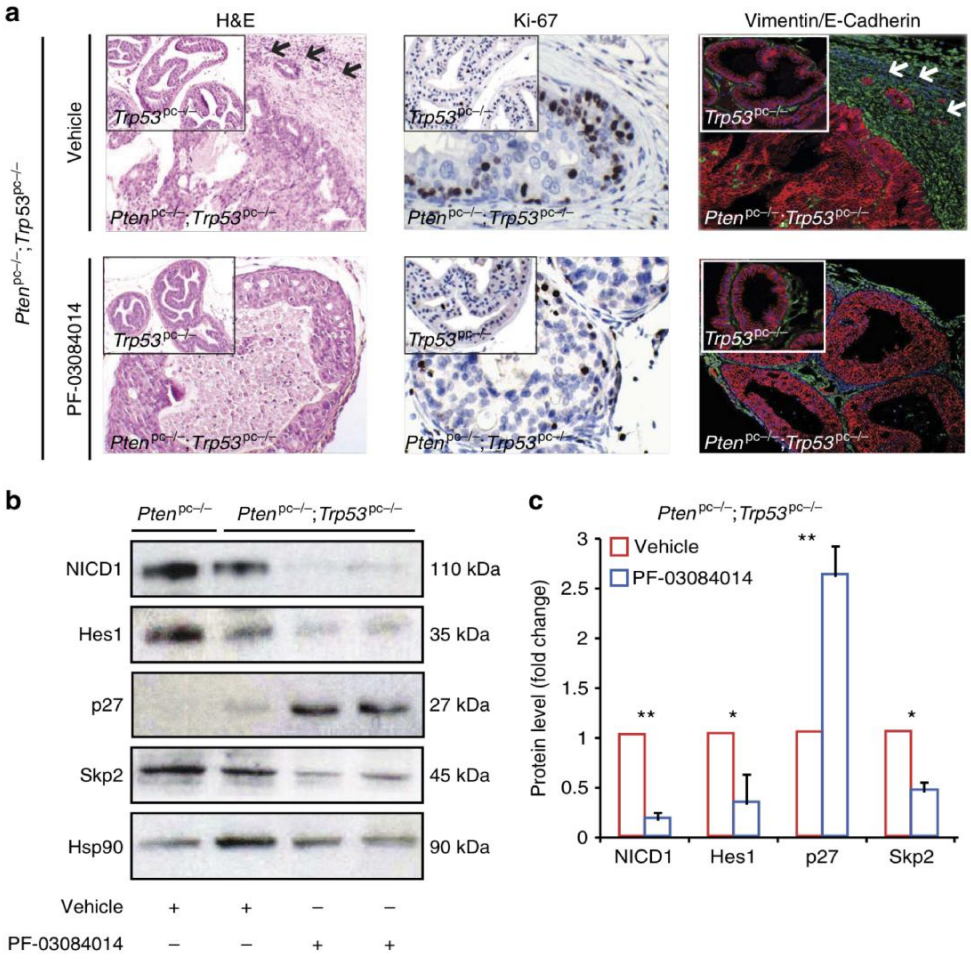

Fig 8. Anti-tumour activity of PF-03084014 in *Pten*$^{pc-/-}$; *Trp53*$^{pc-/-}$ prostate tumours. (**a**) Representative H&E, Ki-67 and Vimentin/E-Cadherin immunofluorescence stainings of *Pten*$^{pc-/-}$; *Trp53*$^{pc-/-}$ prostate tumours treated with either vehicle or PF-03084014. White arrow shows an invasive area of epithelial tumour cells infiltrating the tumour stroma. Insets represent H&E, Ki-67 and Vimentin/E-Cadherin staining in *Trp53*$^{pc-/-}$ normal prostates treated with either vehicle or PF-03084014. (**b**) WB on AP extracts from *Pten*$^{pc-/-}$; *Trp53*$^{pc-/-}$ tumours showing the effect of PF-03084014 on Notch1 signalling. (**c**) Quantification of b. Values are expressed as mean±s.e.m. *P<0.05; **P<0.01 by Student's t-test.

pigmentation phenotype, an indicator of the activity of the compound *in vivo* (Fig 7b)[71,72].

Guided by the results obtained in the *Pten*$^{pc-/-}$ mice, we further aimed to determine the efficacy of g-secretase inhibitor in more advanced and aggressive model of prostate tumours. We sought this aim by taking an advantage of *Pten*$^{pc-/-}$; *Trp53*$^{pc-/-}$ mice that fully develop invasive and aggressive prostate tumours and are also reported to be resistant to major

conventional therapies available in clinic for PCa[52]. Mice were treated for 5 weeks starting at 15 weeks of age when the tumours were invasive. Notably, *Pten*$^{pc+/+}$ and *Trp53*$^{pc-/-}$ mice that do not develop any prostatic lesions were also included in this trial to determine any potential negative effect of PF-03084014 in normal-like prostate tissues and also in *Trp53*-null background[52]. At the end of the treatment mice were euthanized and prostates were resected

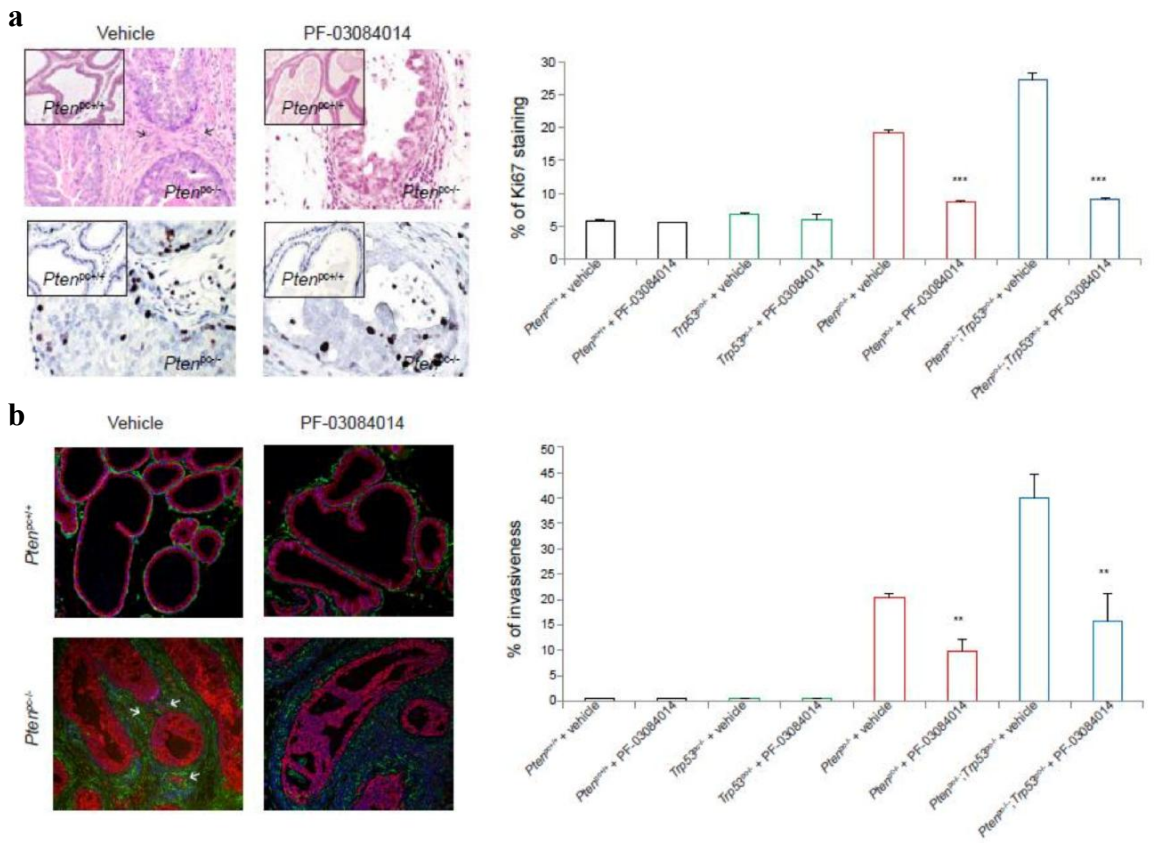

Fig 9. Anti-proliferative effect of PF-03084014 in mouse tumours without affecting normal-like tissues. (**a**) Representative H&E and Ki67 staining images of *Pten*$^{pc+/+}$ (inset) and *Pten*$^{pc-/-}$ tumours treated with vehicle and PF-03084014 (left panel). Arrows in black indicating stroma-infiltrating epithelial-tumour cells. Quantification of Ki67 in mice of indicated genotypes (right panel). Magnification 20x and 40x respectively (n=5). (**b**) Representative IF images for Vimentin/E-Cadherin staining in *Pten*$^{pc+/+}$ and *Pten*$^{pc-/-}$ tumours treated with vehicle and PF-03084014. White arrows indicate stromal-invasion of tumour cells. Right panel quantification of percentage of tumours with invasive prostate glands in mice of indicated genotypes. Magnification 10x (n=5). **P<0.01; ***P<0.001 by Student's t-test.

for analysis. While PF-03084014 treatment did not have any effect on prostatic epithelium of *Pten*$^{pc+/+}$ and *Trp53*$^{pc-/-}$ mice, *Pten*$^{pc-/-}$; *Trp53*$^{pc-/-}$ tumours showed significant decrease in percentage of invasive glands as detected by Haematoxylin and Eosin (H&E) staining and immunofluorescence (IF) staining for Vimentin (stromal marker)/ E-cadherin (Epithelial

marker) (Fig 8a and Fig 9a, b). The reduction in aggressiveness was accompanied by decreased tumour cell proliferation measured by Ki67 staining (Fig 8a and Fig 9a, b). Of importance, we also observed a decrease in focal invasion in *Pten*$^{pc-/-}$ tumours of 15 weeks of age upon treatment with PF-03084014, suggesting that targeting Notch pathway can restrict focal and complete tumour invasiveness (Fig 8a and Fig 9a, b). In line with the results from *Pten*$^{pc-/-}$trials, treatment of *Pten*$^{pc-/-}$; *Trp53*$^{pc-/-}$ tumours with PF-03084014 also showed increase in p27 protein levels and decrease in skp2 protein (Fig 8b, c).

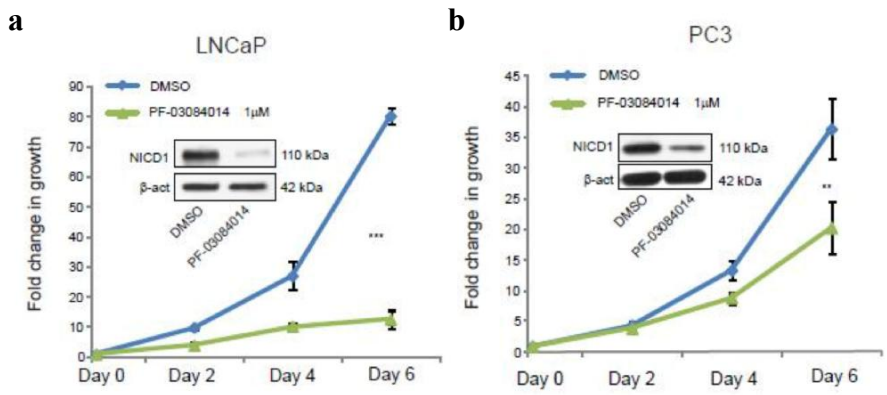

Fig 10. Anti-proliferative effect of PF-03084014 in human PCa cell lines. (**a**) Growth curve of LNCaP cells treated either with DMSO or PF-03084014. (**b**) Growth curve of PC3 cells treated either with DMSO or PF-03084014. Values are expressed as mean ± SEM. **p<0.01; ***p<0.001 by Student's t- test.

Finally, to validate our results in human samples we used LNCaP and PC3, two *PTEN*-deficient metastatic human PCa cell lines and treated them with varying doses of PF-03084014. Treatment with PF-03084014 showed significant cell growth arrest in agreement with recent evidence[73] and trial conducted in *Pten*$^{pc-/-}$ and *Pten*$^{pc-/-}$; *Trp53*$^{pc-/-}$ mice (Fig 10).

Taken together, our preclinical trials support the notion of using g-secretase inhibitor for treating prostate cancers with loss of PTEN which can be beneficial both at early and late stage of tumorigenesis. Having demonstrated the role of Notch pathway and the advantages of pharmacologically targeting it, we wanted to further investigate the molecular mechanism behind the activation of Notch pathway in PTEN-deficient tumours.

Loss-of-PTEN triggers upregulation ADAM17 that subsequently activates Notch pathway in PCa. Notch pathway activation is a tightly regulated process that relies on a hierarchically ordered proteolytic cascade[57,68]. Activation of Notch pathway involves

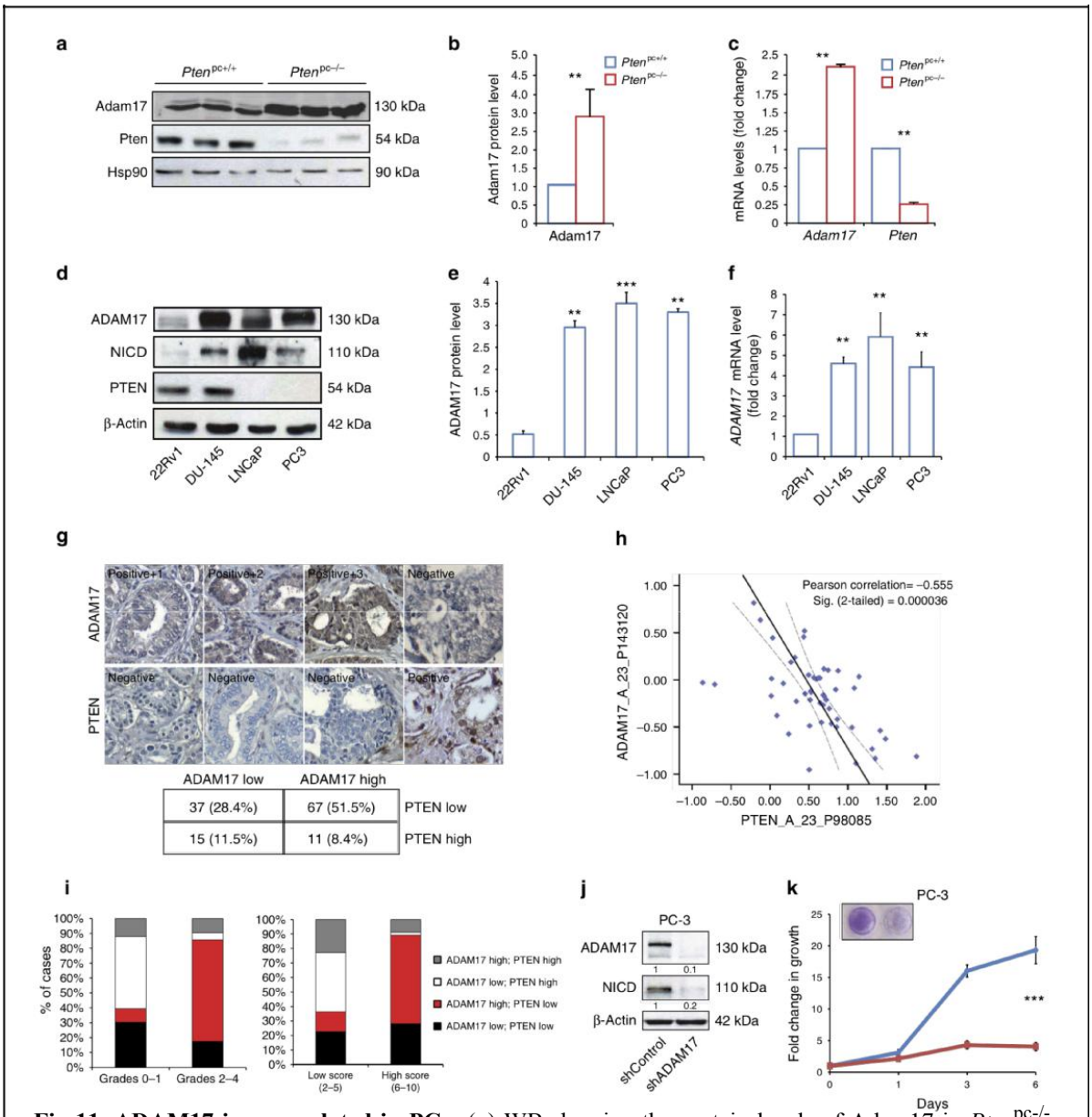

Fig 11. ADAM17 is upregulated in PCa. (**a**) WB showing the protein levels of Adam17 in *Pten*$^{pc-/-}$ tumours compared with *Pten*$^{pc+/+}$ WT prostates. (**b**) Quantification of **a** (n=3). (**c**) Adam17 and Pten mRNA levels in both *Pten*$^{pc+/+}$ prostates and *Pten*$^{pc-/-}$ tumours. (**d**) WB showing the protein levels of ADAM17, NICD and PTEN in different PCa cell lines. (**e**) Quantification of ADAM17 of d. (**f**) ADAM17 mRNA levels in different PCa cell lines. (**g**) ADAM17 and PTEN staining on human prostate cancer tissue microarray (TMA). Table showing correlation between ADAM17 and PTEN staining quantification. Data of two different TMA were combined (total no. of samples=130). (**h**) Inverse correlation between the mRNA levels of PTEN and ADAM17 in human prostate cancers. (**i**) Bar graphs representing the correlation of ADAM17 and PTEN levels with tumour grade and Gleason score. (**j**) WB for ADAM17 and NICD1 in PC3 cells infected with either an shRNA control or shADAM17. (**k**) Growth curve of PC3 cells infected with either an shRNA control or shADAM17. Values are expressed as mean±s.e.m. **Po0.01; ***Po0.001 by Student's t-test.

generation of intracellular NICD1 domain that is cleaved and released by g-secretase enzyme complex. This proteolytic cleavage follows and requires the initial extracellular cleavage of full-length Notch receptor by ADAM metalloproteases[74]. Since ADAM metalloprotease are essential for g-secretase enzyme complex to cleave the NICD1 domain, we

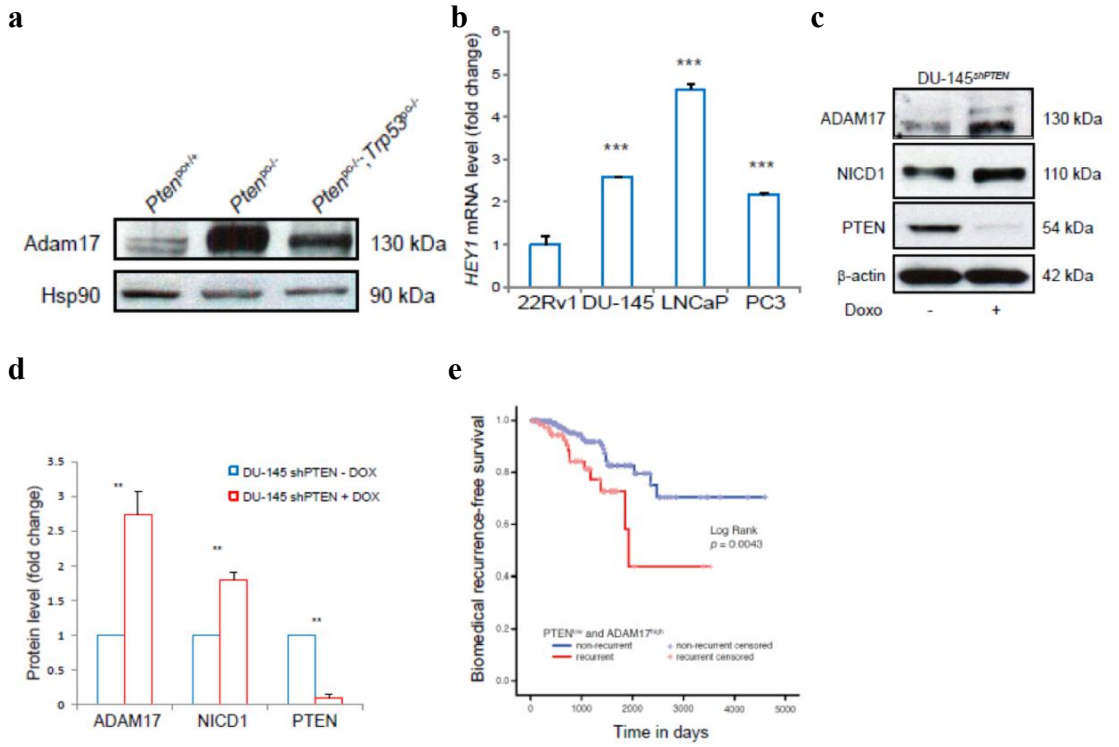

Fig 12. Loss of PTEN regulates ADAM17 expression. (**a**) WB showing the protein levels of Adam17 in *Pten*$^{pc+/+}$ WT prostate, *Pten*$^{pc-/-}$ and *Pten*$^{pc-/-}$; *Trp53* $^{pc-/-}$ prostate tumours. (**b**) HEY1 mRNA levels in different PCa cell lines. (**c**) WB showing the levels of ADAM17, NICD and PTEN in DU-145^{shPTEN} cell line treated with Doxycycline (Dox). (**d**) Quantification of **c**. (**e**) Kaplan-Meier curve showing that prostate cancer patients with low levels of *PTEN* and high levels of *ADAM17* have a worse prognosis. Values are expressed as mean ± SEM. **p<0.01; ***p<0.001 by Student's t-test.

determined the status of ADAM17 metalloprotease. ADAM17 is a metalloprotease involved in NOTCH activation, both in a ligand-dependent and independent manner. Since the ligand-independent activation of NOTCH is strongly correlated with ADAM17 abundancy, we checked the levels of Adam17 in our mouse models. We observed a significant upregulation of Adam17 at both mRNA and protein levels in *Pten*$^{pc-/-}$ tumours (Fig 11a-c) and protein levels in *Pten*$^{pc-/-}$; *Trp53*$^{pc-/-}$ tumours (Fig 12a). Similarly, ADAM17 was upregulated by mRNA and protein levels in human prostate cancer cell lines with functional loss of PTEN in either one

(DU-145) or both (LNCaP and PC3) alleles (Fig 11d-f). This increase in ADAM17 levels was also associated with increase in the levels of NICD1 (WB) (Fig 11d and e) and Notch1 target gene Hairy/Enhancer-of-split related YRPW motif protein (*HEY1* by RT-PCR) (Fig 12b).

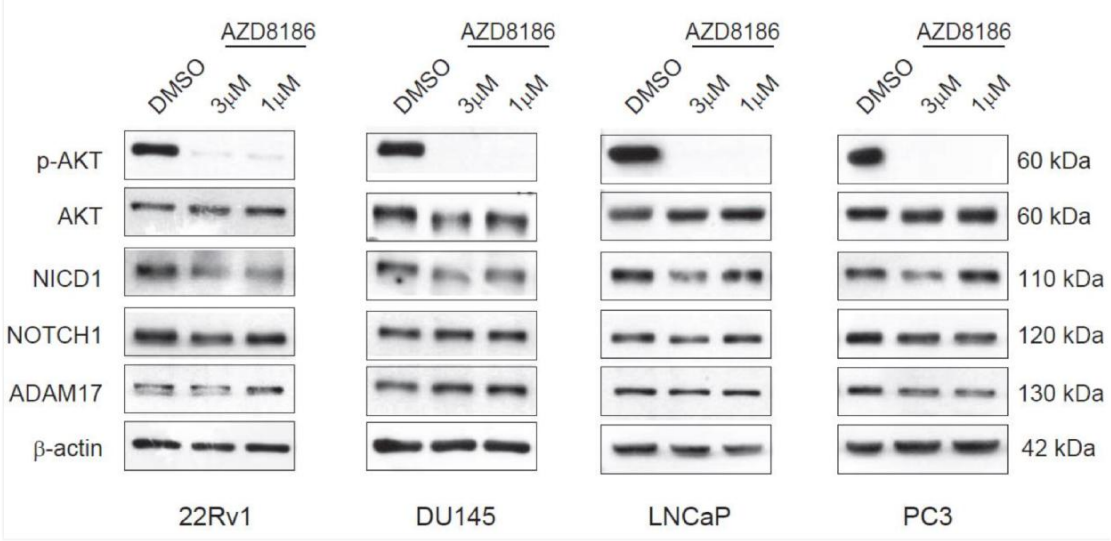

Fig 13 Activation of Notch signalling pathway in PTEN-deficient cells is PI3K/AKT-independent. WB analysis in human PCa cell lines 22Rv1, DU145, LNCaP and PC3 showing protein levels of p-AKT, total AKT, NICD1, NOTCH1 and ADAM17 upon treatment with DMSO and PI3K inhibitor, AZD8186.

Consistent with our mouse models and human cell lines data, we induced genetic inactivation of *PTEN* using shRNA in DU-145 cell line that led to an increase in the expression of ADAM17 and NICD1 levels (Fig 12c and d). To fortify our results with clinical relevance, we next checked the correlation between the protein levels of PTEN and ADAM17 in two independent tissue microarrays (TMAs) comprising of 130 cases in total of human PCa. We performed IHC stainings for ADAM17 and PTEN and analysed the samples for positivity and negativity based on the intensity. Our analysis revealed that majority of the samples displaying low levels of PTEN were stained positively for ADAM17 and vice versa (Fig 11g with P=0.039511). Given that loss of PTEN also triggered upregulation of *ADAM17* mRNA levels we asked whether the inverse correlation between ADAM17 and PTEN is also applicable at the gene expression level. Indeed, our bioinformatic analysis confirmed the inverse correlation between gene expression levels of *PTEN* and *ADAM17* in prostate tumours (Fig 11h). Importantly, while

targeting Notch pathway showed anti-tumour response, we aimed to determine how much does this inverse correlation of low levels and PTEN and high levels of ADAM17 affect the clinical outcome. We observed that low levels of PTEN and high levels of ADAM17 as determined by IHC staining in TMA samples correlated with High Tumour Grade (P<0.0001) and Gleason Score (P<0.0001) (Fig 11i). Moreover, patients with tumours characterized by low levels of *PTEN* and high levels of *ADAM17* ($PTEN^{low}$ $ADAM17^{high}$) had worse clinical outcome (Fig 12e). Altogether, these data indicate that loss of PTEN drives upregulation of ADAM17 and consequently activation of NOTCH pathway.

ADAM17 promoter	
Mouse	Human
RORalpha2	HOXA3
POU6F1(c2)	CUTL1
CUTL1	ATF
RelA	IRF-1
RORalpha1	IRF-7A
C/EBP alpha	AML 1a
POU3F2	AP-1
POU3F2 (N.Oct-5a)	ATF
POU3F2 (N.Oct-5b)	Bach1
POU3F1	C/EBP alpha
AML 1a	CUTL1
AP-1	Elk-1
ATF-2	En-1
Bach1	Evi-1
C/EBP alpha	HNF-4alpha1
CUTL1	HOXA3
Chx10	HIF
E4BP4	IRF-1
Elk-1	IRF-7A
En-1	IK-1
Evi-1	MEF-2a
FAC1	Nrf-2a
FPXJ2	Nkx2-5
XJ2 (long isoform)	Nkx 6-1
FPXL1	Olf-1

Fig 14. List of predicted transcription factors. Top 25 transcription factors predicted to bind the promoter region of both mouse and human *ADAM17* gene based on SABiosciences' proprietary database (DECODE, DECipherment Of DNA Elements). Indicated by font color are other common transcription factors while highlighted is the transcription factor selected.

More importantly, to confirm whether activation of NOTCH pathway is driven by upregulation of ADAM17, we downregulated ADAM17 using short-hairpin RNA. Silencing ADAM17 not only decreased NICD1 protein levels but also reduced the cell proliferation in PC3 cells (Fig 11j, k). These data suggest that PTEN-loss induced NOTCH pathway activation is driven by upregulation of ADAM17.

A transcription factor CUX1 promotes upregulation of *ADAM17* in PTEN-deficient PCa tumours

Our data demonstrates that PTEN-loss leads to increased mRNA and protein levels of ADAM17 that subsequently triggers NOTCH pathway activation. To assess whether this effect was PI3K/AKT dependent, since loss-of-PTEN triggers PI3K/AKT pathway, we treated four human PCa cell lines namely 22Rv1, DU-145, LNCaP and PC3 with PI3K inhibitor, AZD8186. Interestingly, PI3K/AKT inhibition did not affect ADAM17 levels, suggesting that ADAM17 upregulation in PTEN-deficient background was PI3K/AKT-independent (Fig 13). While PTEN-deficiency results in upregulation of ADAM17 (both mRNA and protein) independently of PI3K/AKT, what leads to transcriptional upregulation of ADAM17 still remained elusive. We therefore looked for the transcription factor (TF) that could regulate ADAM17 expression in PTEN-deficient tumour cells.

As both human and mouse data pointed that this mechanism remains conserved, we screened for TFs in SABiosciences' proprietary database (DECODE, DECipherment Of DNA

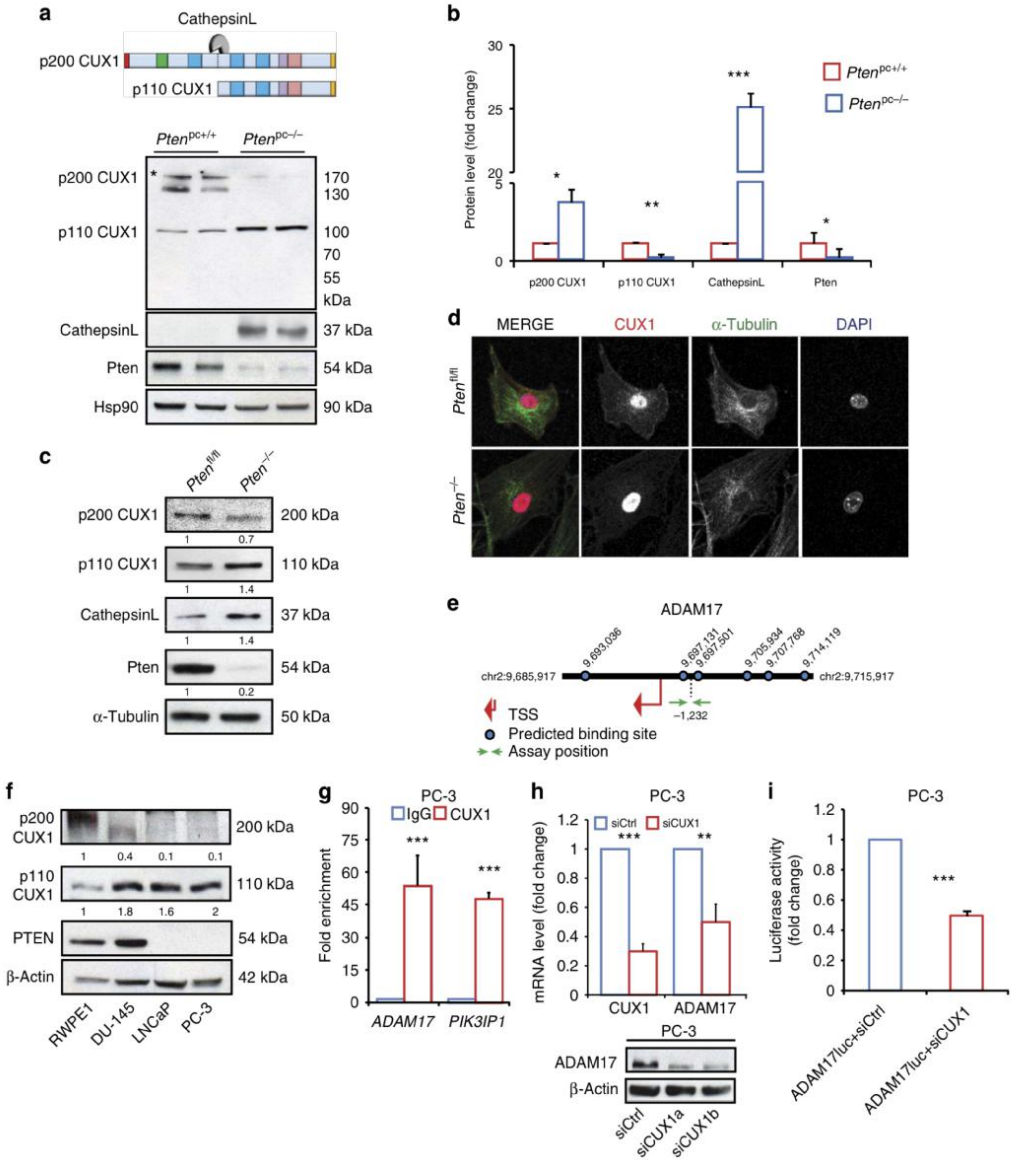

Fig 15. CUX1 regulates ADAM17 expression in prostate tumour. (**a**) Schematic representation of the full-length CUX1 (p200 CUX1) and its oncogenic isoform (p110 CUX1). WB for p200 Cux1, p110 Cux1, Pten and CathepsinL in both *Pten*$^{pc+/+}$ prostates and *Pten*$^{pc-/-}$tumours. (**b**) Quantification of **a** (n=3–5). (**c**) WB showing the levels of Cux1, CathepsinL and Pten in both *Pten*$^{fl/fl}$ and *Pten*$^{-/-}$ MEFs. (**d**) IF images showing the localization of Cux1 in both *Pten*$^{fl/fl}$ and *Pten*$^{-/-}$ MEFs. (**e**) Schematic representation of ADAM17. The blue dots indicate the CUX1 predicted binding sites. In green the region where the primers used for the ChIP experiments have been designed. (**f**) CUX1 and PTEN in different PCa cell lines. (**g**) CUX1 ChIP. Graph showing the fold enrichment of ADAM17 and PIK3IP1 (CUX1 target) genes in PC3 cells. (**h**) mRNA levels and WB for CUX1 and ADAM17 in PC3 cells. (i) ADAM17 luciferase activity upon knockdown of CUX1.
Values are expressed as mean±s.e.m. *P<0.05; **P<0.01; ***P<0.001 by Student's t-test.

Elements) that were predicted to bind ADAM17 promoter in both mouse and human. Amongst the predicted TFs, CUX1 was the only validated and conserved TF in both the species (Fig 14).

Intriguingly, evidence exists that a cleaved form of CUX1 protein, from its full-length (p200 CUX1), p110 CUX1 has a potential oncogenic and transcriptional activator role[75]. While transgenic mouse model overexpressing p110 CUX1 develops mammary carcinomas thereby confirming the oncogenic role of this isoform of CUX1[76], we aim to determine the status of

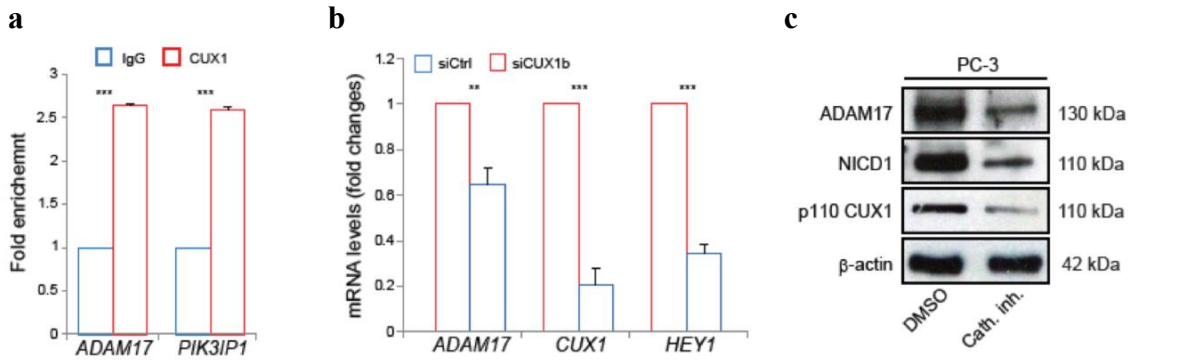

Fig 16. CUX1 p110 isoform regulates ADAM17 expression thereby regulating NOTCH pathway. (**a**) CUX1-ChIP in DU-145 cells. Graph showing the fold enrichment for *ADAM17* and *PIK3IP1*. (**b**) mRNA levels of *ADAM17* and *CUX1* in DU-145 cells transfected with *siCUX1*. (**c**) WB analysis showing the reduction in NICD1 and ADAM17 upon use of CathepsinL inhibitor in PC3 cells. Values are expressed as mean ± SEM. **p<0.01; ***p<0.001 by Student's t-test.

different isoforms of this transcription factor in prostate tumorigenesis. Initially, we determined the expression of CUX1 and its isoforms in *Pten*$^{pc-/-}$ tumours compared to *Pten*$^{pc+/+}$ prostate tissues by western blot analysis. Surprisingly, we observed a marked decrease in the full-length form and a strong increase in oncogenic isoform p110 Cux1 in *Pten*$^{pc-/-}$ tumours. WB (full blot) analysis revealed that the full-length form was mainly expressed in *Pten*$^{pc+/+}$ prostate tissues whereas the cleaved oncogenic isoform p110 Cux1 was predominantly expressed in *Pten*$^{pc-/-}$

tumours (Fig 15a, b). The p110 Cux1 isoform is reported to be a result of a proteolytic cleavage of the full-length p200 Cux1 protein mediated by Cathepsin L and plays a role as transcriptional activator[77]. Therefore, the we next determined the expression of Cathepsin L in *Pten*$^{pc-/-}$tumours. By WB analysis, consistent with p110Cux1 expression levels, Cathepsin L was

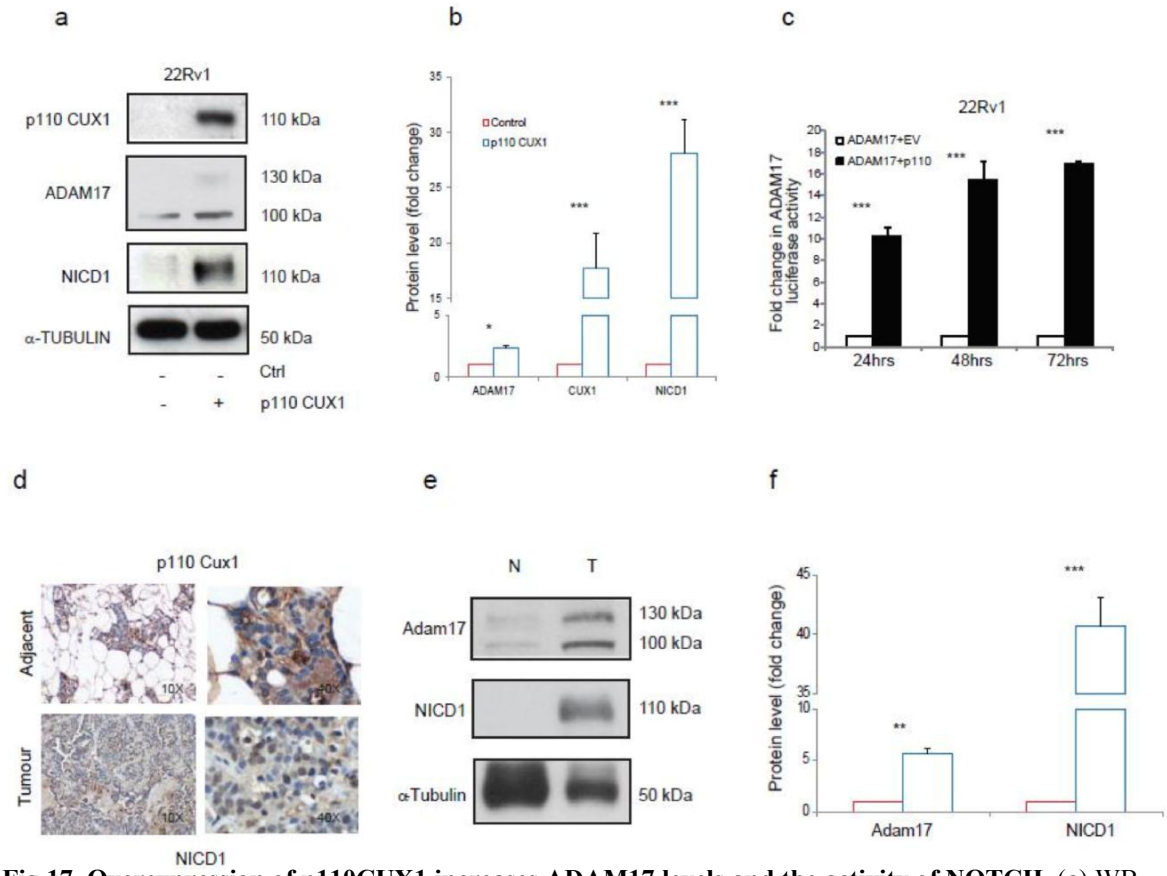

Fig 17. Overexpression of p110CUX1 increases ADAM17 levels and the activity of NOTCH. (**a**) WB analysis in 22Rv1 cells transfected with p110 CUX1 or empty vector. (**b**) Quantification of **a**. (**c**) ADAM17 luciferase activity in cells transfected as in **a** evaluated at different time points. (**d**) Immunohistochemistry for NICD1 in p110 Cux1 breast tumors at both not invasive and invasive stage. Magnification 10x and 40x. (**e**) WB analysis for Adam17 and NICD1 in p110 Cux1 breast cancer and normal mammary glands. (**f**) Quantification of **e**. Values are expressed as mean ± SEM. *p<0.05; **p<0.01; ***p<0.001 by Student's t-test.

markedly upregulated in *Pten*$^{pc-/-}$ tumours compared to *Pten*$^{pc+/+}$ prostate tissues (Fig 15a, b). These data showed that upon loss of *Pten*, Cathepsin L gets upregulated and mediate proteolytic cleavage of Cux1 to its oncogenic form that might be responsible for upregulation of *Adam17* gene expression. These data were further confirmed in *Pten*$^{-/-}$ MEFs by WB and IF analyses (Fig 15c, d). Importantly, p110 CUX1 levels were found to be high in all PCa cell lines, DU-145, LNCaP and PC3, compared to non-tumorigenic immortal cell line RWPE1.

Conversely, the full length p200 CUX1 was barely detected in these PCa cells, while RWPE1 showed high expression of the full-length form of CUX1 compared to its cleaved form (Fig 15f).

Next, we performed Chromatin Immunoprecipitation (ChIP) experiment in PC3 to assess the binding potential of CUX1 on the promoter of *ADAM17* gene (Fig 15e). In agreement with CUX1-binding site prediction, we found that CUX1 strongly binds to the promoter of *ADAM17* gene keeping *PIK3IP1* gene as a positive control wherein CUX1 has been reported to bind on to[78] (Fig 15g). Similar results were obtained in another PCa cell line, DU-145 where CUX1 binds to the promoter of *ADAM17* gene (Fig 16a). Furthermore, to validate our results we used two different small-interfering RNAs (siRNAs) to knockdown the expression of CUX1 to determine its impact on ADAM17 expression levels. Strikingly, knockdown of CUX1 in PC3 strongly reduced the expression of ADAM17 both by mRNA and protein and ADAM17-luciferase activity (FIG 15h, i). Likewise, similar results were obtained in DU-145 cell line (Fig 16b). In line with the siRNA results, treatment of PC3 using a Cathepsin L inhibitor[77], which blocks the conversion of p200 CUX1 to p110 CUX1, decreased the levels of both ADAM17 and NICD1 (Fig 16c).

In sum, our results highlight a novel role of a transcription factor which upon its conversion to its active oncogenic form results in transcriptional activation of ADAM17 and in turn NOTCH pathway activation selectively in PTEN-deficient background.

Overexpression of oncogenic p110 CUX1 activates ADAM17/NOTCH pathway both *in vitro* and *in vivo*

To investigate whether the overexpression of p110 CUX1 can promote activation of NOTCH pathway, we overexpressed p110 CUX1 in 22Rv1 cells. Transient overexpression of p110 CUX1 resulted in increase in ADAM17 and NICD1 protein levels as compared to the Empty vector (EV) (Fig 17a, b). Similarly, overexpression of p110 CUX1 also enhanced the luciferase activity of ADAM17 promoter by nearly 10-folds as compared to the Empty vector (EV) (Fig 17c). As previously published, overexpression of p110 CUX1 in mouse mammary tissue led to development of invasive breast cancer[76], we therefore aimed to determine the levels of Adam17 in these tumour samples. WB and IHC analyses showed enhanced protein expression of Adam17 and NICD1 in mammary tumours compared to adjacent normal mammary glands (Fig 17d-f). Moreover, overexpression of p110 CUX1 in breast carcinoma cell line Hs578T also showed increased expression of *ADAM17* and *HEY1* (NOTCH1 target gene)[79], whereas downregulation of p110CUX1 in the same cells decreased NOTCH1 signalling (Fig 18). In sum, our findings demonstrate that overexpression of p110 CUX1 enhances the transcriptional levels of ADAM17 thereby activating NOTCH1 signalling pathway validating our observations mentioned earlier using different *in vitro* and *in vivo* transgenic mouse models.

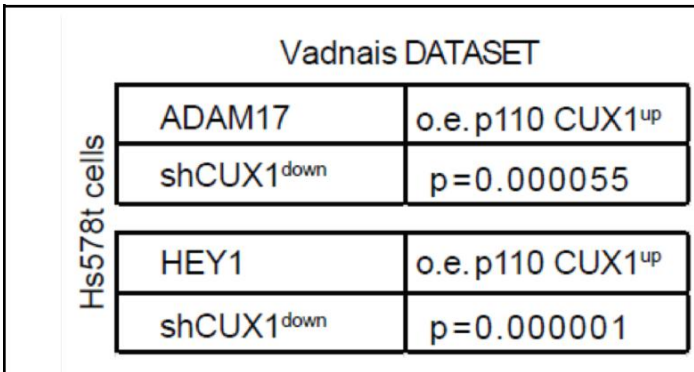

Fig 18. ADAM17 regulation in Hs578T cells before and after overexpression and down regulation of p110 CUX1

3. Discussion

Prostate cancer (PCa) is the second most common cancer-type in men and the fourth most common cancer and cause of cancer-related deaths worldwide[80]. Recent molecular and genetic profiles are performed rapidly in order to categorize various subtypes of cancers and to precisely design targeted-therapy[81]. Despite the significant improvements made in our current understanding of prostate cancer and therapeutic interventions, most advanced, metastatic and recurrent forms of the disease still remain a challenge. Numerous studies have reported that activated NOTCH signalling is associated with advanced[82,83] and metastatic prostate cancer[84,85,86]. However, the mechanism behind NOTCH activation in prostate tumours remained elusive so far. To address this question, we used *Pten*$^{pc-/-}$ and *Pten*$^{pc-/-}$; *Trp53*$^{pc-/-}$mouse models which develop HG-PIN and invasive prostate tumours respectively[52]. In line with human data, we observed an increased NOTCH signalling in the prostate tumours arising
from these mouse models, showing increased g-secretase activity and upregulation of different NOTCH targeted genes (e.g. *Hes1, Ccnd1*). These data suggested that activation of Notch pathway could be a consequence of *Pten*-loss and that this might lead to progression of *Pten*-deficient prostate tumours.

Therefore, to determine the role of Notch signalling in *Pten*-loss driven prostate tumorigenesis, we sought to obtain genetic evidence by generating a combined conditional inactivation of *Pten* and *Notch1* in mouse prostatic epithelia. Strikingly, genetic inactivation of *Notch1* in *Pten*$^{pc-/-}$ mice hampered prostate tumorigenesis at early stage and tumour progression thereafter, by strongly reducing cell proliferation. These results demonstrate that prostate tumours driven by loss-of-*Pten* may in part require the activation of Notch1 signalling. Thus, we envisaged that in therapeutic setting, targeting NOTCH pathway in prostate tumours characterized by loss-of-PTEN might restrict tumorigenesis and subsequently the tumour invasiveness. Indeed, pharmacologically targeting Notch pathway using a g-secretase inhibitor

(GSI), PF-03084014, in *Pten*$^{pc-/-}$ tumours (HG-PIN) and *Pten*$^{pc-/-}$; *Trp53*$^{pc-/-}$ tumours (invasive PCa), dampened tumorigenesis by inhibiting tumour cell proliferation. Notably, both genetic and pharmacological inhibition of Notch signalling were associated with upregulation of a p27-mediated cellular senescence response in both *Pten*$^{pc-/-}$ and *Pten*$^{pc-/-}$; *Trp53*$^{pc-/-}$ tumours. As previously documented, tumours affected by combined loss-of-*Pten* and *Trp53* are insensitive to the majority of clinically available therapies for prostate cancer, such as androgen deprivation and docetaxel[87], and it was therefore surprising to observe that PF-03084014 is highly effective in this tumour background. Activation of p27 in *Pten*-null tumours was associated to decreased Skp2 levels. SKP2 is a known NOTCH target gene and it is a regulator of p27 degradation. Treatment with PF-03084014 in both *Pten*$^{pc-/-}$ and *Pten*$^{pc-/-}$; *Trp53*$^{pc-/-}$ mice, strongly decreased the protein levels of NICD1 and Hes1, thus confirming that the GSI reached its target. These findings are in line with a previous study demonstrating that treatment with a Skp2 inhibitor in a PC3 xenograft mouse model (PC3 cells lack both PTEN and p53) blocks tumorigenesis by upregulating both p27 and senescence[53]. Importantly, SKP2 inhibitors have been associated to several side effects in humans and their clinical development has been currently suspended[88,89,90,91]. Therefore, it is interesting to note that GSIs efficacy is comparable to the one obtained using Skp2 inhibitors but with less toxicity. Our data are also coherent with a recent report demonstrating the efficacy of PF-03084014 in combination with docetaxel, in two human prostate xenograft mouse models[73].

Another major advance of our findings is the characterization of the mechanism that links PTEN-loss to NOTCH activation in prostate cancer. Since upregulation of NOTCH occurred independently of its ligand in PTEN-deficient human prostate cancer cell lines, it remained unclear how aberrant Notch signalling was associated with development and

progression of prostate cancer. Moreover, the activation of g-secretase complex as observed in *Pten*$^{pc-/-}$ tumours, a complex which is activated only upon S2 cleavage mediated by ADAM metalloproteases, pointed towards investigating the role of ADAM17 in PTEN-loss driven PCa. Analysis of proteases involved in activation of Notch signalling has highlighted an increased S2 processing of Notch receptors mediated by the ADAM17 metalloprotease. ADAM17 is involved in the first cleavage of the NOTCH receptor which results in the generation of the NOTCH extracellular domain (NEXT). This allows the subsequent cleavage of NOTCH by the g-secretase complex and translocation of NICD in the nucleus[92,67,74]. Intriguingly, high levels of ADAM17 result in S2 cleavage followed by activation of Notch in a ligand-independent manner[67,74]. In our mouse models and PTEN-deficient human prostate cancer cell lines we observed increase *ADAM17* mRNA levels and an inverse correlation between PTEN and ADAM17, assessed by histological staining in two different TMAs of human prostate cancer. This finding was also confirmed by a bioinformatic analysis of additional human prostate cancer datasets. Furthermore, by knocking down *ADAM17* in PC3 prostate cancer cells, we found decreased

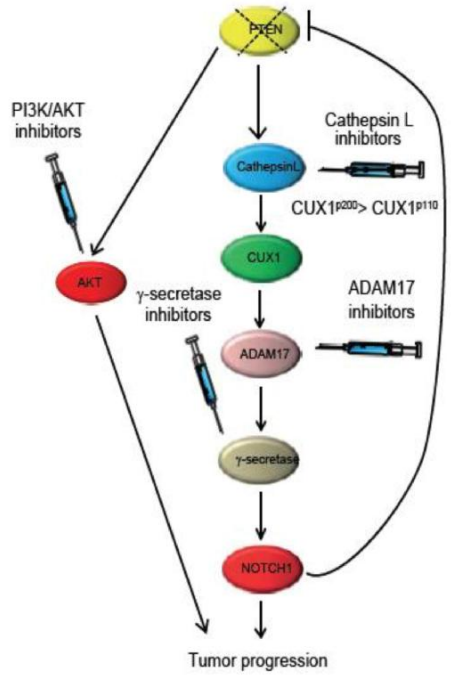

Fig 19. The Model. In prostate tumors with loss of PTEN, the high levels of CathepsinL promote the conversion of p200 CUX1 into its oncogenic isoform p110 CUX1, which in turn binds the promoter of ADAM17 and activates its transcription. ADAM17 then leads to the activation of Notch1 signaling which sustains tumor progression and may further reduce *PTEN* levels. This novel oncogenic network functions independently of PI3K/AKT pathway in the cells having loss of function of PTEN. This study may provide multiple entry points to design novel therapeutic intervention for PCa (e.g. CathepsinL inhibitors, ADAM17 inhibitors, g-secretase inhibitors and AKT inhibitors).

NOTCH1 signalling along with impaired cell proliferation. Altogether, these data confirmed that NOTCH activation in PTEN-deficient cells is a consequence of ADAM17 up-regulation.

While the regulation of NOTCH1 activity by ADAM17 has been extensively investigated[92,57], the regulation of ADAM17 itself is a lesser-known phenomenon. Various studies on transcriptional factors involved in the up-regulation of ADAM17 have shown that under specific conditions, such as hypoxia, ADAM17 expression is up-regulated by different transcription factors[93,94,95]. In this study, we found that CUX1 was the only transcription factor conserved in both mouse and human predicted to bind to *ADAM17*. Multiple isoforms of CUX1 have been identified out of which two are ubiquitously expressed. One is the full-length p200 CUX1, known to function as a transcriptional repressor[96], while the other one is a proteolytically cleaved p110 CUX1 isoform, often regarded as transcriptional initiator and found to be overexpressed in multiple cancers[75]. While p200 CUX1 is known to transiently bind to DNA, the p110 isoform can strongly bind to the promoter region of different genes thereby positively regulating their transcription[97]. In *Pten*-null prostate tumours and human cancer cells, we found manifold increase in p110 CUX1 isoform and an undetectable level of p200 CUX1 when compared to the control. In our ChIP analysis, we also found several fold-increase in binding of CUX1 to the promoter region of *ADAM17* in prostate cancer cell lines, similar to PIK3IP1, a known target of CUX1[78]. Furthermore, knockdown and over-expression of *CUX1* in PCa cells also affected the levels of ADAM17, validating CUX1 as transcription activator of ADAM17. This has been also found *in vivo* in a different mouse model where over-expression of p110 CUX1 is associated to NOTCH activation. Collectively, our observations demonstrate that PTEN-loss promotes the activation of NOTCH signalling by upregulating the levels of p110 CUX1 that in turn promotes the transcription of ADAM17 (Supplementary Fig. 8). This may happen through an enhanced proteolytic activity of Cathepsin L, as shown in our study, or additional mechanisms such as unidentified proteases or non-coding RNAs that may

lead to either the cleavage or stabilization of p110 CUX1 mRNA. The results presented in this work strengthen the potential therapeutic benefits of targeting γ -secretase in prostate cancer and provide a rationale for stratifying patients that may be more responsive to this treatment due to loss of PTEN that mediates activation of NOTCH signalling.

4. Methods and materials

Mice

Pten$^{loxP/loxP}$, *Pten*$^{loxP/loxP}$; *Notch1* $^{loxP/loxP}$, *Notch1* $^{loxP/loxP}$, *Trp53* $^{loxP/loxP}$ and *Pten*$^{loxP/loxP}$; *Trp53* $^{loxP/loxP}$ mice (Jackson laboratory) were crossed with PB-Cre4 transgenic mice to generate prostate-specific knockout of *Pten*, *Pten*; *Notch1*, *Notch1*, *Trp53* and *Pten*; *Trp53* respectively[52]. All mice were maintained under specific pathogen-free conditions in the animal facilities of the IRB institute, and the experiments were performed according to the state guidelines and approved by the local ethical committee. g-secretase inhibitor PF-03084014, used for all the pre-clinical trials in a cohort of *Pten*$^{pc-/-}$ and *Pten*$^{pc-/-}$; *Trp53* $^{pc-/-}$ mice (8 and 15 weeks of age respectively), was synthesized and provided by *Pfizer*. g-secretase inhibitor, PF-03084014, was dissolved in 10% Methyl cellulose solution in water prepared as follows:

1. Heat about 1/3 of the required volume of water to at least 80 °C.
2. Add the methyl cellulose powder (Sigma Aldrich – 09963) to the hot water with agitation.
3. Agitate the mixture until the particles are thoroughly wetted and evenly dispersed.
4. For complete solubilisation, the remainder of the water is then added as cold water or ice to lower the temperature of the dispersion. Once the dispersion reaches the temperature at which that particular methyl cellulose product becomes water soluble, the powder begins to hydrate and the viscosity increases. Solution should be cooled to 0-5 °C for 20-40 min.
5. Continue agitation for at least 30 min. After the proper temperature is reached add g-secretase inhibitor, PF-03084014, to prepare the drug as per the need for treatments *in vivo*.

Mice undergoing treatment were administered control vehicle or therapeutic dosage of PF-03084014 (100mg/kg/twice-a-day) by oral gavage on a Monday through Friday schedule for a

total of 20 days. Mice were monitored for any suffering of distress or weight loss by measuring total body weight of mice biweekly and monitoring the behavioural changes every day for a total of 4-weeks of treatment. Upon completion of study, mice were euthanized by CO_2 asphyxiation and tissues were procured for histological analysis, mRNA analysis and protein analysis.

Autopsy and Histopathology

Animals were autopsied, and all tissues were examined regardless of their pathological status. Normal and tumour tissue samples were fixed in 10% neutral-buffered formalin (Thermo Scientific, Cat No. 5701) for 24-36 hrs after which the Formalin was removed under running tap water and the tissues were kept in either 1x PBS or 70% Ethanol solution until to process. Tissues were processed by ethanol dehydration and embedded in paraffin according to standard protocols. For the normal sized tissues (most of the prostate samples were processed using the following steps:

Program steps:

1. Ethanol 70% - 10 mins (20 mins for bigger tisssues)
2. Ethanol 80% - 10 mins (20 mins for bigger tisssues)
3. Ethanol 95% - 10 mins (15 mins for bigger tisssues)
4. Ethanol 95% - 10 mins (15 mins for bigger tisssues)
5. Ethanol 100% - 10 mins (20 mins for bigger tisssues)
6. Ethanol 100% - 10 mins (20 mins for bigger tisssues)
7. Ethanol 100% - 10 mins (10 mins for bigger tisssues)
8. Xylol - 15 mins (30 mins for bigger tisssues)
9. Xylol - 10 mins (Same time of processing for the bigger tissues too)
10. Xylol - 10 mins (Same time of processing for the bigger tissues too)

11. Paraffin - 35 mins (Same time of processing for the bigger tissues too)
12. Paraffin - 35 mins (Same time of processing for the bigger tissues too)

Sections (5µm) were prepared for antibody detection and Haematoxylin and Eosin (H&E) staining (C0303, Diapath) and (C0363, Diapath) respectively. To evaluate evidence of invasion, sections were cut at 20µm intervals and H&E stained. Slides were prepared containing three to five of these interval sections.

g-secretase assay

γ-Secretase assays using the recombinant human Notch and Amyloid precursor protein substrates Notch100-Flag and APP-C100-Flag were performed as previously reported[98,99,100]. Membrane proteins were extracted from *Pten*$^{pc+/+}$ and *Pten*$^{pc-/-}$ null mice prostate samples in 50 mM HEPES (pH 7.0) with 1% CHAPSO. The protein content in the extracts was normalized by BCA and incubated in 0.2% (wt/vol) CHAPSO, 50 mM HEPES (pH 7.0), 150 mM NaCl, 5 mM $MgCl_2$ and 5 mM $CaCl_2$ and incubated at 37°C for 4 h with 1 µm substrate, 0.1% (wt/vol) phosphatidylcholine and 0.025% (wt/vol) phosphatidylethanolamine. The generated products AICD (Amyloid Intracellular C-terminal Domain) -Flag and NICD (Notch Intracellular Domain) -Flag were analyzed by Western blot and detected with Flag-specific M2 antibody (Sigma-Aldrich).

MEF production and cell culture

Primary MEFs were obtained from individual embryos of *Pten*$^{loxP/loxP}$ genotype from a pregnant mouse at 13.5 days post-coitum. The embryos were harvested from the embryonic sac and the head, limbs, tail and internal organs such as foetal livers (Red dotted immature organs) were dissociated. These embryos were further chopped in 15-20 µl Trypsin-EDTA and were kept in the incubator at 37^{o}C with 5% CO_2 for 20-25 mins. Upon incubation, the trypsin

over the chopped embryos was deactivated using DMEM with 10% FCS and 1% Pen/Strep and the chopped embryos were transferred to a 10mm Petri dish and kept in the incubator. 24 hrs post-seeding, media was changed over the MEFs and were further incubated for additional 2 days. Once the MEFs are ready either they can be freezed using 10% DMSO solution in FCS (Freezing media) or can be plated for infection. Primary *Pten*$^{lox/lox}$ MEFs were infected with retroviruses expressing either pMSCV-CRE-PURO-IRES-GFP or pMSCV-PURO-IRES-GFP for 48 hrs and selected with Puromycin at a concentration of 3 µg ml^{-1}. 293t cells nearly 2x10^{6} were plated in 10mm dish and were transfected using the above-mentioned plasmids (5µg) with Pcl-Eco (1µg) as a helper and transfection was performed using Jetprime solutions and protocol as per manufacturer instructions.

PTEN WT (RWPE-1, 22Rv1) human prostate cell lines and heterozygous or homozygous loss of PTEN function prostate cancer cell lines (DU-145, LNCaP and PC3) were obtained from ATCC and were cultured in RPMI (supplemented with 10% FCS and 1% Pen/Strep) according to the manufacturer instructions.

Proliferation and senescence assays

Proliferation assay in MEFs was performed by plating 10^4 cells per well of 24-well plate in triplicate while that in human PCa cell lines was performed by plating 1-2 x 10^4 cells per well of 24-well plate in triplicate. Cells were treated with vehicle (DMSO) control, AZD8186 (PI3K inhibitor, Astrazeneca) at 3µM and 1µM and g-secretase inhibitor (Dissolved in DMSO only for *in vitro* studies) at aforementioned concentrations. Cell proliferation was monitored on days 0, 2, 4 and 6 whereby cells were fixed for 15mins in a solution of 10% buffered formalin (Thermo Scientific, Cat No. 5701) washed with PBS (pH7.2) and subsequently stained with 0.01% Crystal violet solution. Excessive staining was removed by washing with distilled water and drying the plates overnight. Crystal violet stained cells were dissolved in 10% acetic acid

solution for 30mins on shaker and the extracted dye was read with a spectrophotometer at 590 nm. Cellular senescence *in vitro* was performed using Senescence β -Galactosidase Staining Kit (Cell signalling, Cat No. 9860s) as per manufacturer instructions.

siRNA and shRNA transfection

Human ADAM17-directed shRNA was obtained from Sigma. To prepare lentiviral particles, 293t HEKs were transfected using Jetprime transfection reagents (Polyplus transfection) as per manufacturer instructions. PC3 cells were infected with the lentivirus from transfected 293t HEKs and were subsequently selected using puromycin (2μg/ml). shRNA:5'CCGGCCTATGTCGATGCTGAACAAACTCGAGTTTGTTCAGCATCGACATAGGTTTTTG 3' (Clone ID: NM_003183.3-2002s1c1).

Human CUX1a sequence: 5' AACAGGAGGACACAAGGCAAAGCUG 3'and CUX1b sequence: 5' CAGGGUUUGUUUAAUACACUCCAUU 3' were custom-siRNA synthesized (Dharmacon). siRNA transfection was performed using Jetprime transfection reagents (Polyplus transfection) as per manufacturer instructions.

Western Blotting and histology

Human tissue microarray (TMA) were purchased from Biomax, Inc (PR8011A and PR483B). The antibodies used for IHC analysis and western blot (WB) were anti-activated Notch1 (Abcam) (IHC), Cleaved Notch1 (Val 1744) (Cell Signaling Technology; 1:250 dilution), Notch1 (D1E11) (Cell Signaling Technology; 1:1000) (WB), PTEN (Cell Signaling Technology; 1:1000) (WB), PTEN (51-2400; Invitrogen) (IHC), Ki67(Clone SP6; Lab Vision) (IHC), HSP90 (Cell Signaling Technology; 1:1000), ADAM10 (Abcam; 1:1000), ADAM17 (Abcam; 1:1000) (IHC/WB), CathepsinL (Abcam; 1:1000) (WB) , CUX1 a.a. 1300 (Millipore, 1:2500) and CUX1 a.a. 861 (Millipore; 1:1000) (WB), Skp2 (Santa Cruz; 1:500) (WB), p27

(Santa Cruz; 1:500) (WB), Hes1 (Santa Cruz; 1:500) (WB), c-Myc (Santa Cruz; 1:500) (WB), p21 (Santa Cruz; 1:500) (WB), β-actin (Sigma; 1:5000) (WB).

Immunohistochemistry protocol (IHC)

- **Deparaffinization**

  1. 5’ OTTIX plus solution (Diapath, Cat No. X0076)
  2. 5’ OTTIX plus solution (Diapath, Cat No. X0076)
  3. 5’ OTTIX shaper solution (Diapath, Cat No. X0096)
  4. 5’ dH_2O

- **Unmasking/ Antigen retrieval**

  - Antigen retrieval step was performed in respective pHs at 1X, pH 8 solution (10X stock solution, Diapath, Cat No. T0090), pH 6 (Citrate) solution (10X stock solution, Diapath, Cat No. T0050) and pH 9 solution (DAKO, High pH antigen retrieval solution 50X, Cat No. K800421-2).
  - Unmasking was performed by immersing the slides in cylindrical jars containing respective pH solutions boiled at 98^oC in water bath.
  - The slides were cooled by removing the jar from water bath to room temperature removing the lid. Wait for 20-25’until the solution is cooled and then remove the slides from the solution/jar.

- **Staining procedure**

  - Mark the slides around the edges of embedded tissue with hydrophobic pen.
  - Wash slides with PBST (0.5% Tween20) 2’ x 2.
  - Add drop-wise to cover the tissue fully with 3% H_2O_2 (30% stock solution, Company: VWR chemicals, Cat no: 23615.248) for 10’.
  - Wash slides with PBST (0.5% Tween20) 2’ x 2.

- Add Protein-Block solution (DAKO Agilent technologies, Cat No. X0909) for 10’ at room temperature.
- Drip off the solution and WITHOUT washing the slides, add 1^{o} antibody at the desired concentration in Antigen-Diluent solution (Life technologies, Cat No. 003118) for 1 hour at room temperature.
- Wash the slides with PBST 2’ x 2.
- Add 2^{o} antibody (Anti-Mouse Vector Laboratories, Cat No. BA-2000 and Anti-Rabbit for all the three in this case, Vector Laboratories, Cat No. BA-1000, 1:200 dilution) in 1xPBS solution for 30’ at room temperature.
- Wash the slides with PBST 2’ x 2.
- Meanwhile, prepare Vectastain ABC solution (Company: Vector laboratories, Cat No. PK-6100) dilution of 1:150 of both Solution A and Solution B in 1xPBS solution and leave the mixture for 30’ incubation at room temperature while waiting for the secondary staining.
- Wash the slides with PBST 2’ x 2. Meanwhile, prepare DAB solution (Company: Vector laboratories, Cat No. SK-4105. One drop of Chromogen in 1ml of Diluent solution).
- Add the DAB solution for 4’ and immediately was the slides with PBST 2’ x 2.
- Add Haematoxylin solution for 2’ and immediately after wash the slides with tap water.

Perform the back-solutions procedure.

Back-solutions procedure

1. 2’ OTTIX plus solution (Cat No. X0076, Diapath)
2. 2’ OTTIX plus solution (Cat No. X0076, Diapath)

3. 2’ OTTIX shaper solution (Cat No. X0096, Diapath)
4. Mount the stained slides with mounting media and gently place coverslip. Avoid bubbles.

Add mounting media on the top of the slides and place the coverslips and give a gentle tap to remove all the bubbles.

Haematoxylin and Eosin staining (H&E)

Deparaffinization procedure was performed in the beginning as mentioned in IHC protocol above. Upon Deparaffinization the H&E staining was performed as detailed below:

- **Staining procedure**
    - Stain the slide with Haematoxylin solution (Diapath, Cat no. C0303) for 6-7 mins.
    - Wash the slide with dH_2O for two times.
    - Stain the slides with Eosin solution (1% aqueous) for 2-3 mins.
    - Wash immediately with tap water for three times and perform the back steps.

Back-solution procedure was eventually performed as detailed in IHC protocol section.

Add mounting media on the top of the slides and place the coverslips and give a gentle tap to remove all the bubbles.

Chromatin immunoprecipitation assay

Cells were cultured up to a confluence of 90–95% and were cross-linked with 1% formalin (Final concentration) for 10 min followed by addition of glycine (0.125M Final concentration) for 5 min at room temperature on slow swirling shaker. The culture medium was aspirated and the cells were washed twice with ice-cold PBS. Nuclear extracts were sonicated using a Misonix 3,000 model sonicator to sheer crosslinked DNA to an average fragment size of ~500 bp. The sonicated samples were centrifuged at 12’000 rcm for 10mins at $4^{o}C$ and

aliquoted. g-bind Plus sepharose beads (GE healthcare) were washed using 1x PBS thrice followed by rinsing with ChIP Dilution buffer. Sonicated chromatin was incubated for overnight at 4 °C with g-bind Plus sepharose beads (GE healthcare) conjugated with either anti-CUX1 antibody (Santa Cruz; 200 µg/0.1ml) or IgG antibody (Millipore) by incubating overnight at 4 °C on a rotor. Approximately, 5ml (1% of the total volume of samples used for ChIP) of sonicated-centrifuged samples were separated to be used as Input (like housekeeper). Upon overnight incubation, beads were washed thoroughly using following procedure:

- **Low Salt** buffer wash on rotor (Twice for 5 mins followed by centrifugation no more than 300 rpm).
- **High Salt** buffer wash on rotor (Once for 5 mins followed by centrifugation no more than 300 rpm).
- **Lithium Chloride (LiCl)** buffer wash (Once for 5 mins followed by centrifugation no more than 300 rpm).
- **TE** buffer wash (Twice for 5 mins followed by centrifugation no more than 300 rpm).

The chromatin was eluted from the beads, and crosslinks were removed by incubation at 65 °C for 5 h in Elution buffer. DNA was then purified using the QIAquick PCR Purification Kit (Qiagen, Cat No. 12643). The ChIP primers for ADAM17 EpiTect ChIP qPCR Primer Assay For Human ADAM17, NM_003183.4 (-)02Kb (Qiagen) and PIKChIP1f sequence: 5’ GAGGAAGGAAGGTACTGAACC 3’ and PIKChIP1r sequence: 5’CCTGTAACTAAGACATTTATCAGC 3’. ChIP qPCR was performed using KAPA SYBR FAST ABI qPCR Master Mix solution (KAPA Biosystem) on Step One Real-Time PCR systems (Applied Biosystems). Primers for ADAM17 used in the ChIP experiments were

designed using the SABiosciences' proprietary database (DECODE, DECipherment Of DNA Elements).

Buffers used for this protocol were as follows:

- **ChIP Dilution buffer (Final concentrations)**:

  0.01% SDS

  1.1% Triton X-100

  1.2mM EDTA

  16.7mM Tris-HCl (pH 8.1)

  167mM NaCl

- **Low Salt buffer (Final concentrations)**:

  0.1% SDS

  1% Triton X-100

  2mM EDTA

  20mM Tris-HCl (pH 8.1)

  200mM NaCl

- **High Salt buffer (Final concentrations)**:

  0.1% SDS

  1% Triton X-100

  2mM EDTA

  20mM Tris-HCl (pH 8.1)

  500mM NaCl

- **LiCl buffer (Final concentrations)**:

  0.25M LiCl

  1% IGEPAL-CA630 (NP-40)

  1% Deoxycholic acid

1mM EDTA

10mM Tris-HCl (pH 8.1)

- **TE buffer (Final concentrations)**: 1mM EDTA

  10mM Tris-HCl (pH 8.1)

- **Elution buffer (Final concentrations)**:

  10µl of 10% SDS

  10µl of 1M $NaHCO_3$ (Stored at -20)

  80µl H_2O

  4µl of 5M NaCl

- **Proteinase K. solution to add to Elution buffer (Final concentrations)**:

  4µl of 0.5M EDTA

  8µl of 1M Tris-HCl (pH 6.5)

  1µl of Proteinase K solution

  To a total of 104µl of Elution buffer add 13µl of proteinase K solution.

Quantitative real-time PCR

Quantitative real-time PCR was performed on RNA extracted from cells and respective tissues samples using Trizol (Ambion Life Technologies, Cat No. 15596026).

a. **RNA extraction protocol**: Tissues were homogenised in 500µl of Trizol reagent using 1.5ml Pre-sterilized pestle (Axygen, Cat No. PES- 15-B-SI) and the homogenised samples were incubated at room temperature for 5 mins. Similarly, cells grown in cultures as monolayers were scraped in 500µl of Trizol reagent followed by 5 mins incubation at room temperature. Upon incubation, 100µl of Chloroform (Sigma-

Aldrich, Cat No. C2432) was added and the samples were vortexed for 10-15 secs and incubated at room temperature for 2-3 mins. Samples were centrifuged at no more than 12'000 RCF for 15 mins at 4^{o}C to observe the phases (Lower red, Phenol-chloroform intermediate phase and colourless upper aqueous phase). The RNA is present in the upper phase which is carefully transferred to a new Eppendorf without disturbing the other two phases. Thereafter, 250µl of Isopropanol (2-propanol, Sigma-Aldrich, Cat No. I9516) was added to the upper phase and mixed well using a pipette. The samples were incubated at room temperature for 10 mins followed by centrifugation at no more than 12'000 RCF for 10 mins at 4^{o}C. This allows the formation of white pellet at the bottom of the tube which is washed in 500µl of 75% Ethanol twice separated by centrifugation at 7'500 RCF for 5 mins at 4^{o}C. Finally, the pellet is allowed to dry which is dissolved in DEPC-water of appropriate volume.

b. **Complementary DNA and RT-PCR preparation**: cDNA was prepared from 1µg of RNA using SuperScript III First-Strand Synthesis SuperMix (Invitrogen, Cat No. 11752-050) as per manufacturer instructions. The cDNA samples were further diluted (Dilution rate: 1:2) before to use it for the RT-PCR. See Supplementary Table 2 for list of primers used for qRT-PCR. Quantitative Real-time PCR was performed using KAPA SYBR FAST ABI qPCR Master Mix solution (KAPA Biosystem) on Step One Real-Time PCR systems (Applied Biosystems). Following was the preparation of the respective primer mixes:

1. Forward primer: 1.5 µl of 2µM intermediate stock (Prepared by diluting 1:50 primer stock of 100 µM concentration)
2. Reverse primer: 1.5 µl of 2µM intermediate stock
3. DEPC-water: 1µl
4. SyBR Green solution: 5µl

5. cDNA per well: 1µl (1:2 diluted)

Correlation Analysis

Correlation between gene-expression-derived values in the principle-component analysis PCa data sets was done using Pearson correlation test, which estimates a correlation value ‘‘r’’ and a significance p value ($r > 0 < 1$, direct correlation; $r < 0 > 1$, inverse correlation). Correlation was also performed in TMA staining evaluation using the estimated percentage of positively stained cells. Correlation analyses Pearson r was calculated to assess potential positive ($r > 0$) or negative ($r < 0$) linear correlations between gene expression levels of PTEN and ADAM17, and PTEN and HES1 in the primary tumor biopsies (n=49) comprised in the Grasso human PCA dataset (GSE35988). Two tailed p-values smaller than 0.05 were considered significant

Gene Expression Profiling

Gene expression profiling (GEP) was done using the MouseRef-8 v2.0 Expression BeadChip (Illumina, San Diego, CA, USA), following the manufacturer’s protocol. Arrays were read on an Illumina HiScanSQ system. Data were first extracted with the Illumina GenomeStudio software and then imported in Genomics Suite 6.4 (Partek Incorporated, Saint Louis, MO USA) and quantile normalized. Transcripts with differences in expression were identified by ANOVA. Enrichment analysis was performed using Gene Set Enrichment Analysis (GSEA)[101]. Raw data have been deposited in National Center for Biotechnology Information’s Gene Expression Omnibus (GEO) and are accessible through GEO accession (GSE76822). GSEA was performed on entire gene list ranked according to fold changes observed between *Pten*$^{pc+/+}$ and *Pten*$^{pc-/-}$ mice and also *Pten*$^{pc-/-}$ and *Pten*$^{pc-/-}$ treated with PF-03084014 mice. Functional analysis was performed on the collapsed gene symbol list using GSEA (Gene Set Enrichment Analysis) with the MSigDB_v4.0 (Molecular Signatures Database)[102] C2-C7

gene-sets. Gene-sets with FDR <0.25 and Normalized Enriched Score[103] higher than 1.25 or lower than -1.25 were considered significantly enriched. The VILIMAS_Notch_Targets[104] gene set include 52 genes up-regulated in bone marrow progenitors by constitutively active NOTCH1. Pearson correlation was used to study the association among genes in terms of gene expression. Analyses were performed using the R environment (R Studio console; RStudio, Boston, MA, USA). A p-value <0.05 was considered statistical significant.

Secrete-Pair Dual Luminescence Assay

Cells were co-transfected with ADAM17 promoter reporter clone (HPRM15027, Genecopoeia) along with control vector (pXJ Vector) and p110 CUX1 (pXJ p110). Media from these transfected cells from at different specified time points were collected after changing the media post-transfection. The secreted luciferase (GLuc and SEAP) was measured and analysed as per the manufacturer's guide (SPDA-D010, Genecopoeia).

Immunofluorescence analysis

- **Deparaffinization**
  5. 5' OTTIX plus solution (Diapath, Cat No. X0076)
  6. 5' OTTIX plus solution (Diapath, Cat No. X0076)
  7. 5' OTTIX shaper solution (Diapath, Cat No. X0096)
  8. 5' dH_2O
- **Unmasking/ Antigen retrieval**
  - For Vimentin and E-Cadherin: 1X pH 9 solution (DAKO, High pH antigen retrieval solution 50X, Cat No. K800421-2).
  - Unmasking was performed by immersing the slides in cylindrical jars containing pH 9 solution and boiled at 98^{o}C in water bath.

- Cool the slides by removing the jar from water bath to room temperature and remove the lid. Wait for 20-25'until the solution is cooled and then remove the slides from the solution/jar.

- **Staining procedure**
  - Mark the slides around the edges of embedded tissue with hydrophobic pen.
  - Wash slides with PBST (0.5% Tween20) 2' x 2.
  - Add Protein-Block solution (DAKO Agilent technologies, Cat No. X0909) for 10' at room temperature.
  - Add Biotinylated anti-mouse (Vector Laboratories, Cat No. BA-2000) to block unspecific binding of anti-mouse E-Cadherin antibody on mouse tissue which also gave non-specific background for 20' at room temperature.
  - Drip off the solution and WITHOUT washing the slides, add 1^{o} antibody in Antigen-Diluent solution (Life technologies, Cat No. 003118) for 1 hour at room temperature.
  - Concentration of respective primary antibodies is as below:

    Rabbit anti-Vimentin: 1:350 (Abcam, Cat No. ab92547)

    Mouse anti-E-Cadherin: 1:400 (BD Biosciences, Cat No. 610181)
  - Wash the slides with PBST 2' x 2.
  - Add 2^{o} antibody (Alexa Fluor 594 anti-mouse from Invitrogen, Cat No. A11005 and Alexa Fluor 488 anti-rabbit from Life technologies, Cat No. A11008, both at 1:200 dilution) in 1xPBS solution for 30' at room temperature.
  - Wash the slides with PBST 2' x 2.
  - Lastly, the samples were incubated with mounting media with DAPI (Vectashield, Cat no. H-1200).

Immunofluorescence images were acquired on a Leica TCS SP5 confocal microscope, using a 40X/1.25 N.A. objective (Leica HCX PL APO lambda blue 40X/1.25 oil UV). Several fields of views were acquired with tiling scan function, in order to get an area of 1000um x1000um. Image analysis was performed measuring total fluorescence of transcription factor both in nuclear and cytoplasmic region, with a customized pipeline in CellProfiler software[103]. Images for tissue samples stained for Vimentin/E-cadherin were acquired on a Leica TCS SP5 confocal microscope using 10X/1.25 oil

Statistical Analysis

For each independent *in vitro* experiment, at least three technical replicates were performed with an exception in western blot analysis. In the *in vitro* experiments, data groups were assessed for normal distribution and Student's t test was performed for paired-comparison. The *n* values represent the number of mice used for the study of genetically engineered mouse model analysis and pre-clinical trials using PF-03084014.

Data analysis was performed using a two-tailed unpaired Student's t test. Values are expressed as mean ± SEM (*$p<0.05$; **$p<0.01$; ***$p<0.001$).

5. References:

1. American Cancer Society. Cancer Facts & Figures 2017. *Cancer Facts Fig. 2017* 1 (2017). doi:10.1097/01.NNR.0000289503.22414.79
2. Jemal, A. *et al.* Cancer Statistics, 2009. *CA. Cancer J. Clin.* **59,** 225–249 (2009).
3. Leitzmann, M. F. & Rohrmann, S. Risk factors for the onset of prostatic cancer: Age, location, and behavioral correlates. *Clinical Epidemiology* **4,** 1–11 (2012).
4. Wolf, A. M. *et al.* American Cancer Society Guideline for the Early Detection of Prostate Cancer Update 2010. *Cancer Journal, The* **60,** 70–98 (2010).
5. Lu-Yao, G. L. *et al.* Outcomes of localized prostate cancer following conservative management. *JAMA* **302,** 1202–9 (2009).
6. True, L. *et al.* A molecular correlate to the Gleason grading system for prostate adenocarcinoma. *Proc. Natl. Acad. Sci. U. S. A.* **103,** 10991–6 (2006).
7. Sartor, A. O. *et al.* Evaluating Localized Prostate Cancer and Identifying Candidates for Focal Therapy. *Urology* **72,** (2008).
8. Shen, M. M. & Abate-Shen, C. Molecular genetics of prostate cancer: new prospects for old challenges. *Genes Dev.* **24,** 1967–2000 (2010).
9. Bostwick, D. G., Liu, L., Brawer, M. K. & Qian, J. High-grade prostatic intraepithelial neoplasia. *Rev. Urol.* **6,** 171–9 (2004).
10. Shappell, S. B. *et al.* Prostate Pathology of Genetically Engineered Mice: Definitions and Classification. The Consensus Report from the Bar Harbor Meeting of the Mouse Models of Human Cancer Consortium Prostate Pathology Committee. in *Cancer Research* **64,** 2270–2305 (2004).
11. Abdulkadir, S. A. *et al.* Conditional loss of Nkx3.1 in adult mice induces prostatic intraepithelial neoplasia. *Mol. Cell. Biol.* **22,** 1495–503 (2002).
12. Abate-Shen, C. *et al.* Nkx3.1; Pten mutant mice develop invasive prostate adenocarcinoma and lymph node metastases. *Cancer Res.* **63,** 3886–3890 (2003).
13. Trotman, L. C. *et al.* Pten dose dictates cancer progression in the prostate. *PLoS Biol.* **1,** (2003).
14. Ellwood-Yen, K. *et al.* Myc-driven murine prostate cancer shares molecular features with human prostate tumors. *Cancer Cell* **4,** 223–238 (2003).
15. Grignon, D. J. Unusual subtypes of prostate cancer. *Modern Pathology* **17,** 316–327 (2004).
16. Humphrey, P. A. Diagnosis of adenocarcinoma in prostate needle biopsy tissue. *J. Clin. Pathol.* **60,** 35–42 (2007).
17. Abate-Shen, C. & Shen, M. M. Molecular genetics of prostate cancer. *Genes and Development* **14,** 2410–2434 (2000).
18. Bubendorf, L. *et al.* Metastatic patterns of prostate cancer: An autopsy study of 1,589 patients. *Hum. Pathol.* **31,** 578–583 (2000).
19. Logothetis, C. J. & Lin, S. H. Osteoblasts in prostate cancer metastasis to bone. *Nature Reviews Cancer* **5,** 21–28 (2005).
20. Aceto, N. *et al.* Circulating tumor cell clusters are oligoclonal precursors of breast cancer metastasis. *Cell* **158,** 1110–1122 (2014).
21. Aceto, N., Toner, M., Maheswaran, S. & Haber, D. A. En Route to Metastasis: Circulating Tumor Cell Clusters and Epithelial-to-Mesenchymal Transition. *Trends in Cancer* **1,** 44–52 (2015).
22. Liu, W. *et al.* Copy number analysis indicates monoclonal origin of lethal metastatic prostate cancer. *Nat. Med.* **15,** 559–565 (2009).
23. Salmena, L., Carracedo, A. & Pandolfi, P. P. Tenets of PTEN Tumor Suppression. *Cell* **133,** 403–414 (2008).

24. Mulholland, D. J. *et al.* Pten loss and RAS/MAPK activation cooperate to promote EMT and metastasis initiated from prostate cancer stem/progenitor cells. *Cancer Res.* **72,** 1878–1889 (2012).
25. Ding, Z. *et al.* SMAD4-dependent barrier constrains prostate cancer growth and metastatic progression. *Nature* **470,** 269–276 (2011).
26. Bertrand, F. E., McCubrey, J. A., Angus, C. W., Nutter, J. M. & Sigounas, G. NOTCH and PTEN in prostate cancer. *Adv. Biol. Regul.* **56,** 51–65 (2014).
27. BIGNER, S. H., MARK, J., MAHALEY, M. S. & BIGNER, D. D. Patterns of the early, gross chromosomal changes in malignant human gliomas. *Hereditas* **101,** 103–113 (1984).
28. Li, J. *et al.* PTEN, a putative protein tyrosine phosphatase gene mutated in human brain, breast, and prostate cancer. *Science (80-.).* **275,** 1943–7 (1997).
29. Steck, P. A. *et al.* Identification of a candidate tumour suppressor gene, MMAC1, at chromosome 10q23.3 that is mutated in multiple advanced cancers. *Nat. Genet.* **15,** 356–362 (1997).
30. Di Cristofano, A., Pesce, B., Cordon-Cardo, C. & Pandolfi, P. P. Pten is essential for embryonic development and tumour suppression. *Nat. Genet.* **19,** 348–355 (1998).
31. Stambolic, V. *et al.* Negative regulation of PKB/Akt-dependent cell survival by the tumor suppressor PTEN. *Cell* **95,** 29–39 (1998).
32. Manning, B. D. & Cantley, L. C. Supplemental Data AKT / PKB Signaling : Navigating Downstream. *Cell* **129,** 1261–1274 (2007).
33. Zoncu, R., Efeyan, A. & Sabatini, D. M. MTOR: From growth signal integration to cancer, diabetes and ageing. *Nature Reviews Molecular Cell Biology* **12,** 21–35 (2011).
34. Song, M. S., Salmena, L. & Pandolfi, P. P. The functions and regulation of the PTEN tumour suppressor. *Nature Reviews Molecular Cell Biology* **13,** 283–296 (2012).
35. WEINHOUSE, S., WARBURG, O., BURK, D. & SCHADE, A. L. On Respiratory Impairment in Cancer Cells. *Science (80-.).* **124,** 267–272 (1956).
36. Eguez, L. *et al.* Full intracellular retention of GLUT4 requires AS160 Rab GTPase activating protein. *Cell Metab.* **2,** 263–272 (2005).
37. Sundqvist, A. *et al.* Control of lipid metabolism by phosphorylation-dependent degradation of the SREBP family of transcription factors by SCFFbw7. *Cell Metab.* **1,** 379–391 (2005).
38. Li, X., Monks, B., Ge, Q. & Birnbaum, M. J. Akt/PKB regulates hepatic metabolism by directly inhibiting PGC-1?? transcription coactivator. *Nature* **447,** 1012–1016 (2007).
39. Horie, Y. *et al.* Hepatocyte-specific Pten deficiency results in steatohepatitis and hepatocellular carcinomas. *J. Clin. Invest.* **113,** 1774–1783 (2004).
40. Fang, M. *et al.* The ER UDPase ENTPD5 promotes protein N-glycosylation, the Warburg effect, and proliferation in the PTEN pathway. *Cell* **143,** 711–724 (2010).
41. Martin-Belmonte, F. *et al.* PTEN-Mediated Apical Segregation of Phosphoinositides Controls Epithelial Morphogenesis through Cdc42. *Cell* **128,** 383–397 (2007).
42. Song, L. B. *et al.* The polycomb group protein Bmi-1 represses the tumor suppressor PTEN and induces epithelial-mesenchymal transition in human nasopharyngeal epithelial cells. *J. Clin. Invest.* **119,** 3626–3636 (2009).
43. Zhang, J. *et al.* PTEN maintains haematopoietic stem cells and acts in lineage choice and leukaemia prevention. *Nature* **441,** 518–522 (2006).
44. Yilmaz, Ö. H. *et al.* Pten dependence distinguishes haematopoietic stem cells from leukaemia-initiating cells. *Nature* **441,** 475–482 (2006).
45. Guo, W. *et al.* Multi-genetic events collaboratively contribute to Pten-null leukaemia stem-cell formation. *Nature* **453,** 529–533 (2008).

46. Lindsay, Y. *et al.* Localization of agonist-sensitive PtdIns(3,4,5)P3 reveals a nuclear pool that is insensitive to PTEN expression. *J. Cell Sci.* **119,** 5160–5168 (2006).
47. Shen, W. H. *et al.* Essential Role for Nuclear PTEN in Maintaining Chromosomal Integrity. *Cell* **128,** 157–170 (2007).
48. Song, M. S. *et al.* Nuclear PTEN regulates the APC-CDH1 tumor-suppressive complex in a phosphatase-independent manner. *Cell* **144,** 187–199 (2011).
49. Liu, X. S. *et al.* Polo-like kinase 1 facilitates loss of Pten tumor suppressorinduced prostate cancer formation. *J. Biol. Chem.* **286,** 35795–35800 (2011).
50. Muñoz-Espín, D. & Serrano, M. Cellular senescence: From physiology to pathology. *Nature Reviews Molecular Cell Biology* **15,** 482–496 (2014).
51. Alimonti, A. *et al.* A novel type of cellular senescence that can be enhanced in mouse models and human tumor xenografts to suppress prostate tumorigenesis. *J. Clin. Invest.* **120,** 681–693 (2010).
52. Chen, Z. *et al.* Crucial role of p53-dependent cellular senescence in suppression of Pten-deficient tumorigenesis. *Nature* **436,** 725–730 (2005).
53. Lin, H. K. *et al.* Skp2 targeting suppresses tumorigenesis by Arf-p53-independent cellular senescence. *Nature* **464,** 374–379 (2010).
54. Kim, J. *et al.* A mouse model of heterogeneous, c-MYC-initiated prostate cancer with loss of Pten and p53. *Oncogene* **31,** 322–332 (2012).
55. Carver, B. S. *et al.* Aberrant ERG expression cooperates with loss of PTEN to promote cancer progression in the prostate. *Nat. Genet.* **41,** 619–624 (2009).
56. Carracedo, A. & Pandolfi, P. P. The PTEN-PI3K pathway: Of feedbacks and cross-talks. *Oncogene* **27,** 5527–5541 (2008).
57. Bray, S. J. Notch signalling in context. *Nature Reviews Molecular Cell Biology* **17,** 722–735 (2016).
58. D'Souza, B., Miyamoto, A. & Weinmaster, G. The many facets of Notch ligands. *Oncogene* **27,** 5148–5167 (2008).
59. Raya, Á. *et al.* Notch activity acts as a sensor for extracellular calcium during vertebrate left-right determination. *Nature* **427,** 121–128 (2004).
60. Cordle, J. *et al.* Localization of the delta-like-1-binding site in human Notch-1 and its modulation by calcium affinity. *J. Biol. Chem.* **283,** 11785–11793 (2008).
61. Haines, N. & Irvine, K. D. Glycosylation regulates Notch signalling. *Nat. Rev. Mol. Cell Biol.* **4,** 786–797 (2003).
62. Gordon, W. R. *et al.* Structural basis for autoinhibition of Notch. *Nat. Struct. Mol. Biol.* **14,** 295–300 (2007).
63. Weng, A. P. *et al.* Activating mutations of NOTCH1 in human T cell acute lymphoblastic leukemia. *Science* **306,** 269–71 (2004).
64. Parks, A. L. & Curtis, D. Presenilin diversifies its portfolio. *Trends in Genetics* **23,** 140–150 (2007).
65. Sato, T. *et al.* Active γ-secretase complexes contain only one of each component. *J. Biol. Chem.* **282,** 33985–33993 (2007).
66. Struhl, G. & Adachi, A. Requirements for Presenilin-dependent cleavage of notch and other transmembrane proteins. *Mol. Cell* **6,** 625–636 (2000).
67. Kopan, R. & Ilagan, M. X. G. The Canonical Notch Signaling Pathway: Unfolding the Activation Mechanism. *Cell* **137,** 216–233 (2009).
68. Ranganathan, P., Weaver, K. L. & Capobianco, A. J. Notch signalling in solid tumours: A little bit of everything but not all the time. *Nature Reviews Cancer* **11,** 338–351 (2011).
69. Papayannidis, C. *et al.* A Phase 1 study of the novel gamma-secretase inhibitor PF-03084014 in patients with T-cell acute lymphoblastic leukemia and T-cell

lymphoblastic lymphoma. *Blood Cancer Journal* **5,** (2015).
70. Olsauskas-Kuprys, R., Zlobin, A. & Osipo, C. Gamma secretase inhibitors of Notch signaling. *OncoTargets and Therapy* **6,** 943–955 (2013).
71. Schouwey, K. & Beermann, F. The Notch pathway: Hair graying and pigment cell homeostasis. *Histology and Histopathology* **23,** 609–616 (2008).
72. Moriyama, M. *et al.* Notch signaling via Hes1 transcription factor maintains survival of melanoblasts and melanocyte stem cells. *J. Cell Biol.* **173,** 333–339 (2006).
73. Cui, D. *et al.* Notch pathway inhibition using PF-03084014, a γ-secretase inhibitor (GSI), enhances the antitumor effect of docetaxel in prostate cancer. *Clin. Cancer Res.* **21,** 4619–4629 (2015).
74. Bozkulak, E. C. & Weinmaster, G. Selective Use of ADAM10 and ADAM17 in Activation of Notch1 Signaling. *Mol. Cell. Biol.* **29,** 5679–5695 (2009).
75. Ramdzan, Z. M. & Nepveu, A. CUX1, a haploinsufficient tumour suppressor gene overexpressed in advanced cancers. *Nature Reviews Cancer* **14,** 673–682 (2014).
76. Cadieux, C. *et al.* Mouse mammary tumor virus p75 and p110 CUX1 transgenic mice develop mammary tumors of various histologic types. *Cancer Res.* **69,** 7188–7197 (2009).
77. Goulet, B., Truscott, M. & Nepveu, A. A novel proteolytically processed CDP/Cux isoform of 90 kDa is generated by cathepsin L. *Biol. Chem.* **387,** 1285–1293 (2006).
78. Wong, C. C. *et al.* Inactivating CUX1 mutations promote tumorigenesis. *Nat. Genet.* **46,** 33–38 (2014).
79. Vadnais, C. *et al.* Long-range transcriptional regulation by the p110 CUX1 homeodomain protein on the ENCODE array. *BMC Genomics* **14,** 258 (2013).
80. Ferlay, J. *et al.* GLOBOCAN 2012 v1.0, Cancer Incidence and Mortality Worldwide: IARC CancerBase. No. 11 [Internet]. *Lyon, France: International Agency for Research on Cancer.* **11,** http://globocan.iarc.f (2013).
81. Abeshouse, A. *et al.* The Molecular Taxonomy of Primary Prostate Cancer. *Cell* **163,** 1011–1025 (2015).
82. Ross, A. E. *et al.* Gene expression pathways of high grade localized prostate cancer. *Prostate* n/a-n/a (2011). doi:10.1002/pros.21373
83. Bin Hafeez, B. *et al.* Targeted knockdown of Notch1 inhibits invasion of human prostate cancer cells concomitant with inhibition of matrix metalloproteinase-9 and urokinase plasminogen activator. *Clin. Cancer Res.* **15,** 452–459 (2009).
84. Santagata, S. *et al.* JAGGED1 expression is associated with prostate cancer metastasis and recurrence. *Cancer Res.* **64,** 6854–6857 (2004).
85. Zayzafoon, M., Abdulkadir, S. A. & McDonald, J. M. Notch Signaling and ERK Activation Are Important for the Osteomimetic Properties of Prostate Cancer Bone Metastatic Cell Lines. *J. Biol. Chem.* **279,** 3662–3670 (2004).
86. Shou, J., Ross, S., Koeppen, H., De Sauvage, F. J. & Gao, W. Q. Dynamics of Notch expression during murine prostate development and tumorigenesis. *Cancer Res.* **61,** 7291–7297 (2001).
87. Toso, A. *et al.* Enhancing chemotherapy efficacy in pten-deficient prostate tumors by activating the senescence-associated antitumor immunity. *Cell Rep.* **9,** 75–89 (2014).
88. Skaar, J. R., Pagan, J. K. & Pagano, M. SCF ubiquitin ligase-targeted therapies. *Nature Reviews Drug Discovery* **13,** 889–903 (2014).
89. Palumbo, A. *et al.* Bortezomib, doxorubicin and dexamethasone in advanced multiple myeloma. *Ann. Oncol.* **19,** 1160–1165 (2008).
90. Adams, J. The proteasome: a suitable antineoplastic target. *Nat. Rev. Cancer* **4,** 349– 360 (2004).
91. Wang, Z. *et al.* Skp2: a novel potential therapeutic target for prostate cancer. *Biochim.*

Biophys. Acta **1825,** 11–7 (2012).
92. Sulis, M. L., Saftig, P. & Ferrando, A. A. Redundancy and specificity of the metalloprotease system mediating oncogenic NOTCH1 activation in T-ALL. *Leukemia* **25,** 1564–1569 (2011).
93. Szalad, A., Katakowski, M., Zheng, X., Jiang, F. & Chopp, M. Transcription factor Sp1 induces ADAM17 and contributes to tumor cell invasiveness under hypoxia. *J. Exp. Clin. Cancer Res.* **28,** 129 (2009).
94. Charbonneau, M. *et al.* Hypoxia-inducible factor mediates hypoxic and tumor necrosis factor alpha-induced increases in tumor necrosis factor-alpha converting enzyme/ADAM17 expression by synovial cells. *J. Biol. Chem.* **282,** 33714–24 (2007).
95. Li, R. *et al.* High glucose up-regulates ADAM17 through HIF-1β in mesangial cells. *J. Biol. Chem.* **290,** 21603–21614 (2015).
96. Mailly, F. *et al.* The human cut homeodomain protein can repress gene expression by two distinct mechanisms: active repression and competition for binding site occupancy. *Mol. Cell. Biol.* **16,** 5346–5357 (1996).
97. Moon, N. S., Bérubé, G. & Nepveu, A. CCAAT displacement activity involves CUT repeats 1 and 2, not the CUT homeodomain. *J. Biol. Chem.* **275,** 31325–31334 (2000).
98. Cacquevel, M. *et al.* Rapid purification of active γ-secretase, an intramembrane protease implicated in Alzheimer's disease. *J. Neurochem.* **104,** 210–220 (2008).
99. Wu, F. *et al.* Novel gamma-secretase inhibitors uncover a common nucleotide-binding site in JAK3, SIRT2, and PS1. *FASEB J.* **24,** 2464–74 (2010).
100. Alattia, J.-R. *et al.* Mercury is a direct and potent -secretase inhibitor affecting Notch processing and development in Drosophila. *FASEB J.* **25,** 2287–2295 (2011).
101. Thompson, M. A. *et al.* Differential gene expression in anaplastic lymphoma kinase-positive and anaplastic lymphoma kinase-negative anaplastic large cell lymphomas. *Hum. Pathol.* **36,** 494–504 (2005).
102. Liberzon, A. *et al.* Molecular signatures database (MSigDB) 3.0. *Bioinformatics* **27,** 1739–1740 (2011).
103. Carpenter, A. E. *et al.* CellProfiler: image analysis software for identifying and quantifying cell phenotypes. *Genome Biol.* **7,** R100 (2006).
104. Vilimas, T. *et al.* Targeting the NF-kappaB signaling pathway in Notch1-induced T-cell leukemia. *Nat Med* **13,** 70–77 (2007).